UNIVERSITY OF CALIFORNIA,
IRVINE

Carbon Nanotube High Frequency Devices

THESIS

submitted in partial satisfaction of the requirements
for the degree of

Master of Science

in Electrical and Computer Engineering

by

Shengdong Li

Thesis Committee:
Professor Peter J. Burke, Chair
Professor Chen. S. Tsai
Professor Franco De Flaviis

2004

©2004 by Shengdong Li

All Rights Reserved

The thesis of Shengdong Li is approved:

Committee Chair

University of California, Irvine

2004

Table of Contents

List of Figures vi

List of Symbols and Abbreviations ix

Acknowledgements x

ABSTRACT OF THE THESIS xii

Chapter 1 1

Introduction to Carbon Nanotubes 1

1.1 Structure and General Properties 1

1.1.1 Atomic Structure 1

1.1.2 DC Properties 4

1.1.3 AC Properties 6

1.2 Thesis Overview 9

Chapter 2 11

Carbon Nanotube Growth by Catalytic Chemical Vapor Deposition 11

2.1 Development of a CVD System 11

2.1.1 Parts and Accessories 11

2.1.2 Control System 16

2.2 Catalyzed Growth of Carbon Nanotubes on Nanoparticle Catalyst 22

2.2.1 Introduction 22

2.2.2 Aqueous Catalyst Recipe 22

2.2.3 CNT Growth 24

2.2.4 Growth Results and Discussion 28

2.3 Catalytic Growth of Carbon nanotubes on Metal Thin Film Catalyst 37

2.3.1 Motivation 37

2.3.2 Catalyst Patterning and CVD 38

2.3.3 Growth Results and Discussion 38

2.4 Summary and Perspective 41
Chapter 3 42
Top-gated Carbon Nanotube Field Effect Transistor 42
3.1 Self-marked Photolithography 43
3.2 Top-gated CNTFET using silicon nitride as gate dielectric 46
3.2.1 Introduction 46
3.2.2 Why Silicon Nitride 47
3.2.3 Device Fabrication 49
3.2.4 Electrical Measurement and Discussion 52
Chapter 4 55
Carbon Nanotube GHz Devices 55
4.1 Device Fabrication 56
4.1.1 CNT Growth 56
4.1.2 Electrical Contact 56
4.1.3 Device Characterization 56
4.2 LC Resonator Design 57
4.2.1 Test Fixture 59
4.3.2 Device Mounting 59
4.3.3 Equivalent Circuit 60
4.3 Semiconducting CNT Resonator 61
4.3.1 Semiconducting CNT DC Electrical Properties 61
4.3.2. Semiconducting CNT AC Electrical Properties 62
4.3.4. Analysis and Discussion 63
4.4 Metallic CNT Resonator 65
4.4.1 Metallic Nanotube DC Electrical Properties 65
4.4.2 Metallic Nanotube AC Electrical Properties 65
4.4.3. Analysis and Discussion 67

4.5 Conclusion and Future Work 68

Appendix A Nano Furnace Manual 69

Reference 71

LIST OF FIGURES

Figure 1.1 Form a single-walled CNT from a graphene sheet. 2

Figure 1.2 Examples of CNTs with different (n, m) indices. 3

Figure 1.3 Schematic depiction of a capacitively contacted CNT. 7

Figure 1.4 Circuit diagram for a single-walled CNT. 8

Figure 2.1 A photo of the CVD system. 13

Figure 2.2 Drawing of the growth tube. 14

Figure 2.3 Design diagram of the gas control system. 19

Figure 2.4 Circuit diagram for the control electronics. 21

Figure 2.5 Process of patterning aqueous catalyst 24

Figure 2.6 Schematic depiction of CNT growth. 25

Figure 2.7 A representative gas profile 27

Figure 2.8 A representative temperature profile 27

Figure 2.9 AFM images of CNTs grown on nanoparticle catalyst. 31

Figure 2.10 A CNT 320 µm in length. 34

Figure 2.11 A CNT with a buckle. 34

Figure 2.12 A smooth CNT 80 µm in length. 35

Figure 2.13 A CNT bridging a pair of catalyst pattern. 35

Figure 2.14 SEM image of CNTs grown from Ni thin film catalyst. 40

Figure 2.15 TEM image of nanotubes grown from nickel thin film catalyst. 40

Figure 3.1 CNTs contacted using self-marked photolithography. 44

Figure 3.2 Schematic cross section view of top-gated CNT transistor 47

Figure 3.3 Detailed processing steps. 51

Figure 3.4 I-V characteristics of a top-gated CNTFET using silicon nitride gate dielectric. 53

Figure 3.5 I-V characteristics (Vg = 0V) of a top-gated CNTFET. 53

Figure 4.1 SEM image of the metallic single-walled CNT. 58

Figure 4.2 SEM image of the semiconducting single-walled CNT. 58

Figure 4.3 Equivalent circuit for the resonator. 60

Figure 4.4 DC electrical properties of semiconducting CNT.................................... 62
Figure 4.5 Measured S_{11} for semiconducting nanotube resonator. 63
Figure 4.6 DC electrical properties of metallic nanotube. 65
Figure 4.7 Measured S_{11} for metallic nanotube resonator... 66

List of Tables

Table 2.1 Specification of the parts and accessories of Nano Furnace 15

Table 2.2 ON/OFF control of the gas flow in Nano Furnace 18

Table 2.3 Specification of the gases.. 20

LIST OF SYMBOLS AND ABBREVIATIONS

CNT	Carbon nanotube
CVD	Chemical vapor deposition
RF	Radio frequency
FET	Field effect transistor
Z_L	Load impedance
Z_0	Characteristic impedance
S_{11}	Reflection coefficient $S_{11} = \frac{Z_L - Z_0}{Z_L + Z_0}$
L_k	Kinetic inductance (per unit length)
C_E	Electrostatic capacitance (per unit length)
C_Q	Quantum capacitance (per unit length)
R_D	Drude-like resistance or diffusive resistance
Gc	Two terminal conductance of an individual single-walled CNT
Rt	Two terminal resistance of an individual single-walled CNT
R_0	Lower limit of Rt ($R_0 = h/4e^2 \approx 6.5$ kΩ)
SEM	Scanning electron microscope
AFM	Atomic force microscope
TEM	Transmission electron microscope

ACKNOWLEDGEMENTS

This thesis covers my research from June 2002 to Dec 2003 with Professor Peter Burke in the Department of Electrical Engineering and Computer Science at University of California, Irvine. First of all, I would like to express my deepest appreciation for the scientific guidance and support provided by my research advisor, Professor Peter Burke. He taught me many things about electronics, physics and biotechnology. His vast knowledge of various science and engineering disciplines and unmatchable enthusiasm for innovation continue to enhance my own intellectual development.

None of the work in this thesis would have succeeded without the technical support maintained by the entire cast of characters in Integrated Nanosystems Research Facility at UCI over the years. When setting up our own CVD system, I was immensely aided by Jake Hess with his extensive experience in semiconductor industry. And David Romero helped me a lot such as welding and bending of stainless steel tubing. I also want to thank Vu Phan and Qingzhou Xu for the patience in helping me on a number of equipments such as electron beam evaporator SEM and PECVD/RIE.

Additionally, I have enjoyed the happy cooperation among the entire BurkeLab. I was very impressed by Sungmu Kang, Jenny Yu, Lifeng Zheng and Daniel Oh’s enthusiasm and determination in research, which I myself have been trying to emulate. I also appreciate Sungmu’s effort in setting up a number of test tools.

Furthermore, I would like to thank my friends for sharing their knowledge in fabrication and testing: Harrison Chang, Richard Chang, Dawei Wang, Zhiyong Fan and

Yan Le. I would like to express particular gratitude to Sunan Liu. She helped me in LabView programming and encouraged me frequently when I was about to giving up.

Finally, I thank my family for constant support, both moral and financial.

ABSTRACT OF THE THESIS

Carbon Nanotube High Frequency Devices

By

Shengdong Li

Master of Science in Electrical Engineering and Computer Science

University of California, Irvine, 2004

Professor Peter J. Burke, Chair

This thesis highlights the first-ever electrical measurement of carbon nanotube (CNT) devices (transistors and resonators) operating at microwave frequencies. It is divided into three parts: 1) Catalytic growth of CNTs by chemical vapor deposition; 2) Fabrication and measurement of top-gated CNT transistors using silicon nitride as gate dielectric; 3) Fabrication and electrical measurement of microwave devices made of individual single-walled CNTs.

Our work starts with the design and installation of a chemical vapor deposition system for the growth of single-walled CNTs. Then we explore an aqueous catalyst recipe, which is compatible with conventional photoresist and photolithography. The combination of the self-built chemical vapor deposition system and aqueous catalyst recipe has enabled fabrication of ultra long and high quality single-walled CNTs for device applications. We have also investigated the growth of CNTs using metal thin film catalyst.

Carbon nanotubes are then integrated into electrical devices and circuits using a self-marked photolithography. We have demonstrated gating CNT transistors with silicon nitride thin film. The electrical measurement at dc shows that silicon nitride is chemically benign to CNTs.

CNT devices (transistors and resonators) operating at microwave frequencies are realized for the first time. Microwave signal is coupled to individual single-walled CNTs through impedance matching network. By varying the dc back-gate voltage to a semiconducting CNT, the source-drain impedance at 2.6 GHz is modulated and microwave frequency operation of a CNT transistor is thus demonstrated. In contrast, varying the dc back-gate voltage to a metallic CNT has no effect on the microwave source-drain impedance. We find that the ac source-drain impedance differs from the dc source-drain resistance. These experiments indicate the distributed nature of the capacitive and inductive impedances of the CNT/metal contacts and those of CNT itself.

CHAPTER 1

INTRODUCTION TO CARBON NANOTUBES

1.1 Structure and General Properties

Carbon nanotube (CNT) is the latest allotrope of carbon discovered by Ijima in 1991 [1]. Since then, CNTs have been a leading candidate in continued improvement of the performance, speed and density of integrated circuits [2].

1.1.1 Atomic Structure

CNTs can be viewed conceptually as graphene (a single atomic layer of graphite) sheets rolled up into concentric cylinders. The number of sheets is the number of walls and thus CNTs fall into two categories: single-walled CNTs and multiwall CNTs. There are currently three methods to synthesize CNTs: arc discharge [3], [4], laser ablation [5] and chemical vapor deposition [6]. In this thesis, the main focus is single-walled CNTs synthesized by CVD.

The atomic structure of a single-walled CNT is conveniently explained in terms of two vectors Ch and T in Figure 1.1. T is called translational vector, it defines the direction of CNT axis. Ch is called chiral vector, representing the circumference of a CNT. Two carbon atoms crystallographically equivalent to each other were placed together according to: $Ch = n \cdot \mathbf{a1} + m \cdot \mathbf{a2}$, where **a1** and **a2** are the unit vectors of the

2D grapheme sheet. (n, m) indices determine the diameter and chirality of CNTs. Figure 1.2 shows three representative CNTs of different indices. (n, n) tubes from “arm-chair” since the atoms around the circumference are in an arm-chair pattern, as shown in both Figure 1.1 and 1.2 (a). (n, 0) tubes are termed as “zig-zag”, as in Figure 1.2 (b) and the others are chiral, with rows of hexagons spiraling along the nanotube axis, as in Figure 1.2 (c).

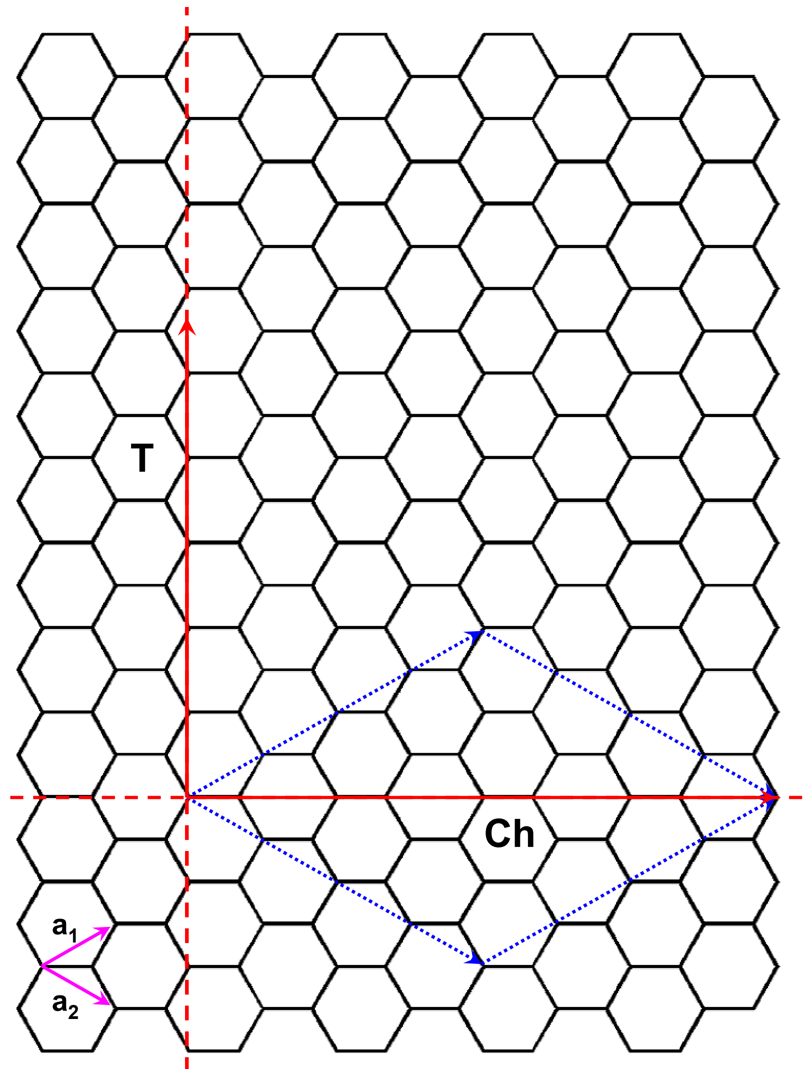

Figure 1.1 Form a single-walled CNT from a graphene sheet.
This example represents a (4, 4) arm-chair CNT, also shown in Figure 1.2 (a).

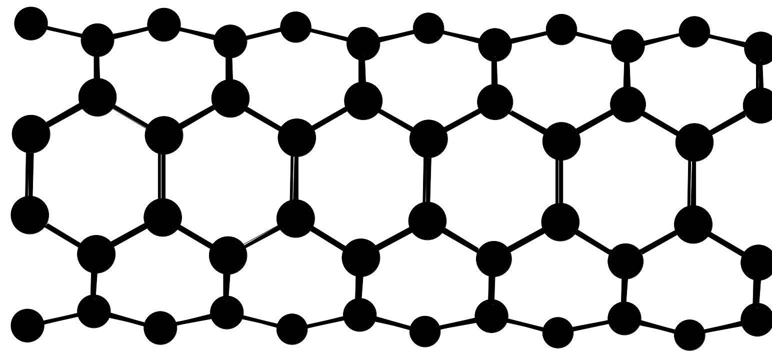

(a) (4, 4) -- armchair

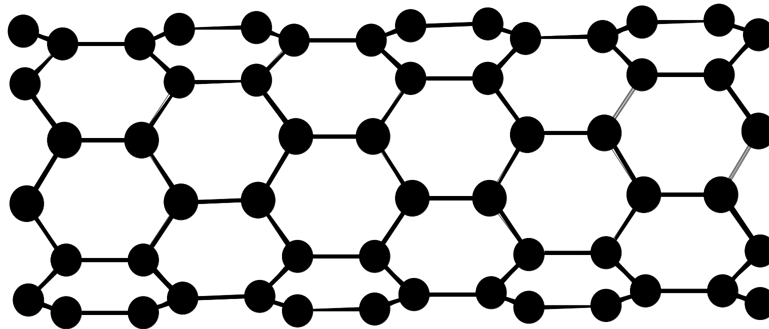

(b) (6, 0) -- zig-zag

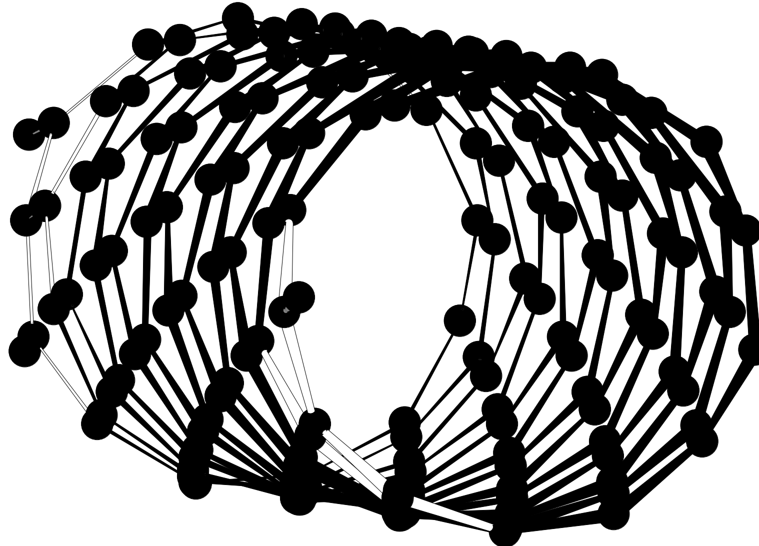

(c) other chirality

Figure 1.2 Examples of CNTs with different (n, m) indices.

1.1.2 DC Properties

Theoretical studies have shown that a single-walled CNT can be either metallic or semiconducting depending on its chirality and diameter [2]. (n, m) nanotubes with $n = m$ (arm-chair) are metallic; for $n - m \neq 3 \times$ integer, the nanotube are semiconducting with band gap proportional to 1/d. For $n - m = 3 \times$ integer, the nanotubes would be quasi-semiconducting, with a small band gap proportional to $1/d^2$. The sensitivity of electrical properties on structural parameters is unique for CNTs, which opens up numerous opportunities in nanotube systems.

First of all, single walled CNTs are 1D quantum systems and the two-terminal conductance is given by Landauer-Buttiker formalism as: $Gc = N \cdot e^2/h \cdot T$, where N is the number of conduction channels in parallel and T is transmission coefficient [7]. For a single-walled CNT, the band structure gives rise to two propagating channels and taking into account the additional spin quanta of electrons, there are four “channels” in total. Therefore, $N = 4$ and $Gc = 4e^2/h \cdot T$, corresponding to a two-terminal resistance $R_C = 1/Gc = h/4e^2 \cdot (1/T)$. In addition, the scattering of charge carriers along the length of CNTs results in a Drude-like resistance, $R_D \propto L_{CNT}$, where L_{CNT} is the length of the CNT. Thus, the total resistance of a single-walled CNT contacted by metal leads on both ends is the sum of these two contributions: $Rt = R_C + R_D$.

If the contact is perfect ($T = 1$) and the CNT is scattering free, charge carriers can move through the nanotube ballistically, we have $Rt = Rc = h/4e^2 \approx 6.5\ k\Omega = R_0$. This lower limit of resistance arises from the mismatch of the number of conduction channels in single-walled CNT and the macroscopic metal leads and is the lower limit. This was first observed for metallic CNTs [8], [9] in 2001. Usually, Rt and Rc are greater than R_0

because T is less than one due to the reflection of charge carriers at the imperfect metal/CNT interface. Rt becomes even greater when there exists energy barriers at the metal/CNT interface, namely, Schottky barriers [10] when CNTs are semiconducting. Schottky barriers have been a long standing problem for silicon and other conventional semiconductors. This problem is circumvented by replacing metal leads with heavy doping in conventional semiconductor industry. However, doping CNTs with nanoscale scale spatial resolution would be a formidable challenge. It is suggested that metal/CNT Schottky barriers might be more easily controlled due to nanoscale geometry and chemical structure of CNTs [11]. Recently, Rt approaching R_0 has been observed for semiconducting CNTs by Javey et al. [12] at room temperature. The undesired surface states and dangling bonds in 2D materials are elegantly circumvented in CNTs by taking advantage of the cylindrical geometry. In addition, the sp^2 hybridyzed chemical bonds of CNTs are typically delocalized, which affords extraordinary charge mobility. Fuhrer group [13] reported a mobility of 79000 $cm^2/V{\cdot}s$ measured from a semiconducting CNT. This value exceeds those for all known semiconductors. Furthermore, the strong covalent bonds give CNTs high mechanical strength and thermal stability and enormous charge carrying capacity [2]. Current density as high as 10^9 A/cm^2 have been reported [14]. Transconductance has been a key parameter in evaluating the performance of a transistor. Despite the fact that CNT FETs are still far from being optimized, a number of groups [15-17] have been reported very encouraging data, both experimentally and theoretically. These works lay the foundation for future ultra high performance, high speed ballistic transistors.

While the large-scale integration of CNT FETs has yet been attained, a variety of primitive functional units such as inverters, logic gates and ring oscillators [18-20] have been realized. Considering the nanometer scale diameter of CNTs, which is determined by chemistry rather than lithography, it should be possible in principle to make extremely high density pure CNT integrated circuits using semiconducting CNTs as the active components (transistors) and metallic CNTs as passive components (interconnects).

On the other hand, localization of charge carriers on the CNTs due to high metal-CNT contact barrier and weak coupling is also useful to construct single electron transistors. Room temperature single electron transistors based on CNTs have been reported in reference [21]. Applying RF/microwave techniques to this field will enable supersensitive and ultra fast analog circuits, which might be useful in future quantum computing.

1.1.3 AC Properties

While the evaluation of CNT devices at dc has been positive, research on directly addressing the dynamic performance of CNTs has just started. One major impediment to applying high frequency signals to CNT FETs is that high impedance exists at the metal/CNT interface. The reflection coefficient is defined as:

$$S_{11} = (Z_L - Z_0) / (Z_L + Z_0) \tag{1.1}$$

where Z_L is the load impedance and Z_0 is the characteristic impedance of the transmission line.

Assuming the real part of this contact impedance is equal to R_0 at dc -- approximately 6.5 kΩ -- S_{11} is almost equal to 1 with respect to a typical 50 Ω

transmission line, which indicates that the entire high frequency electromagnetic signal will be bounced back in effect. The high impedance due to the limited conduction channel of individual CNTs can be overcome in principle by using an array of CNTs, which is definitely a research topic for CNT fabrication technology. Another alternative will be completely circumventing this conduction channel mismatching by coupling the CNT with a capacitive contact [22, 23], as shown in Figure 1.3. Similar approach has been commonly applied to 2D electron gas [24]. A capacitive contact is in principle simple to achieve: any parallel conductive plate close to the CNT will be capacitively coupled to it. At GHz frequencies, this capacitance can behave as a short circuit, allowing efficient (i.e. low-impedance) high-frequency contact to a nanotube. However, for this to be the case, the length of the CNT must be significant, even for parallel plates very close to the nanotube.

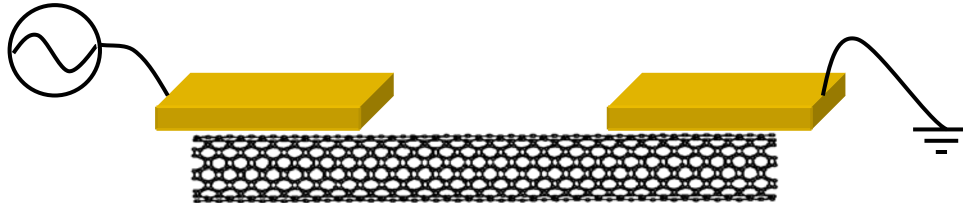

Figure 1.3 Schematic depiction of a capacitively contacted CNT.

In reference [22] and [23], a single-walled CNT has been modeled as a transmission line (Figure 1.4) due to the distributed nature of capacitance and inductance. The distributed circuit elements are:

Kinetic inductance per unit length: $L_k = \dfrac{h}{2e^2 v_F}$ (1.2)

Electrostatic capacitance per unit length: $C_E = \dfrac{2\pi\varepsilon}{\cosh^{-1}(2h/d)} \approx \dfrac{2\pi\varepsilon}{\ln(h/d)}$ (1.3)

Quantum capacitance per unit length: $C_Q = \frac{2e^2}{hv_F}$ (1.4)

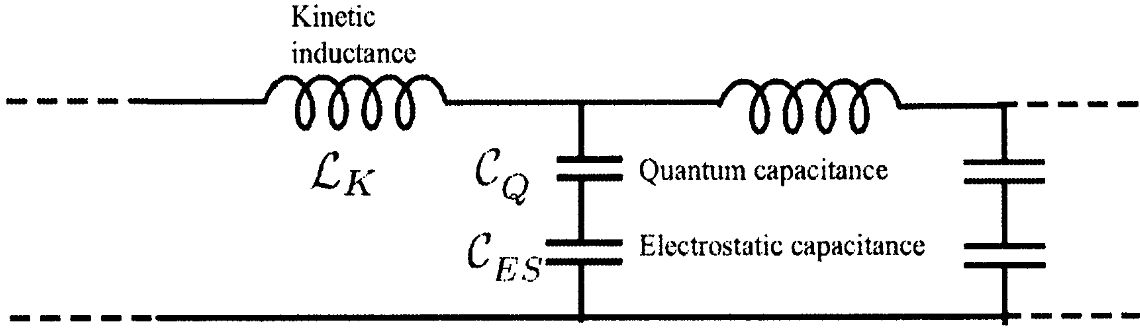

Figure 1.4 Circuit diagram for a single-walled CNT.
Adopted from reference [23].

Plugging all the physical constants and a rough estimation gives the order of magnitude for the three aforementioned parameters: $L_k \approx 10nH/\mu m$, $C_E \approx 50aF/\mu m$ and $C_Q \approx 100aF/\mu m$. The quantization of kinetic energy in the 1D system of single-walled CNT gives rise to the significant inductance which might be working as inductors in future CNT RF integrated circuits. The capacitive coupling between CNT and metal plates is actually very small. To bring the resonance down to GHz frequencies, CNTs of order of 100 μm in length must be grown [22].

This circuit model is of great technological significance in determining the switching speed of CNT based electronic devices, both diffusive and ballistic. On the other hand, the deviation of the measured wave velocity of the CNT transmission line from the Fermi velocity will directly determine the electron-electron interaction in 1D systems, namely, Luttinger liquid behavior [22].

1.2 Thesis Overview

My work begins with the CVD synthesis of single-walled CNTs from lithographically patterned catalyst sites. SEM, AFM and TEM characterization instruments are used extensively. SEM is the primary tool for determining the orientation, location and length of CNTs. AFM is good at measuring the diameter of CNTs. TEM tells us the exact number of walls. CNTs are then integrated into electrical devices of different geometry using a self-marked process. The results of electrical measurement of CNT devices at high frequencies, in particular, appear to be quite encouraging.

The first chapter covers the discovery and general properties of CNTs and gives an overview of this thesis.

Chapter 2 starts with the development of a CVD system. Sophisticated design of the control system to ensure the highest level of security is adopted. Then an aqueous catalyst recipe which is compatible with regular photoresist and conventional photolithography is explored. The combination of the self-built CVD system and aqueous catalyst recipe has enabled fabrication of ultra long and high quality single-walled CNTs. We have also tried metal thin film catalyst and multiwall CNTs are observed to bridge 15 μm apart Ni catalyst pair.

Chapter 3 presents our progress toward making of CNT devices and circuits of high speed, high performance and high density of integration. We propose and demonstrate a process to fabricate top-gated CNT transistors using silicon nitride as the gate dielectric. We find the oxygen-free deposition process of silicon nitride to be more chemically benign to CNTs than those of oxides.

Chapter 4 focuses on the CNT transistors and resonators operating at microwave frequencies. Lumped circuit elements are connected to CNTs to transform the high impedance at the metal/CNT interface. Both individual semiconducting and metallic CNTs are characterized at GHz frequencies. Varying the dc back-gate voltage for a semiconducting CNT varies the source-drain impedance at 2.6 GHz and thus verifying microwave frequency operation of a CNT transistor. In contrast, varying the dc back-gate voltage on a metallic CNT at dc has no effect on the microwave source-drain impedance. We find that the ac source-drain impedance differs from the dc source-drain resistance, which reveals the distributed nature of the capacitive and inductive impedances of the CNT/metal contacts and those of CNT itself.

CHAPTER 2

CARBON NANOTUBE GROWTH BY CATALYTIC CHEMICAL VAPOR DEPOSITION

Catalytic chemical vapor deposition is the most practical method for the development of CNT devices. It is scalable and compatible with integrated circuits and MEMS/NEMS manufacturing processes. CVD allows high specificity of single-walled or multiwall CNTs through appropriate selection of process gasses and catalyst. In this chapter, CNT growth on patterned catalyst sites is described, which forms the foundation for all the work in this thesis. The first section describes the design and setup of a CVD system. Next, an aqueous catalyst recipe using nanoparticles as active catalyst is described. Then, CNT growth on metal thin film catalyst is described. CNTs post CVD are extensively characterized using SEM and AFM.

2.1 Development of a CVD System

2.1.1 Parts and Accessories

Due to the success of this project, this CVD system has been recognized as one of the public fabrication facilities in INRF, nicknamed as “Nano Furance”. Therefore, in the following part of this thesis, this CVD system is generally called as Nano Furnace.

The major parts of Nano Furnace are: a Lindberg furnace combined with a Eurotherm 818P temperature controller/programmer and a 3” growth tube (Quartz), five MKS mass flow controllers, a Tylan RO-28 flow rate controller and a Sensi 360 flammable gas transmitter (with sensor), and controlling electronics and valves, as shown in Figure 2.1. The Eurotherm 818P controller/programmer allows PID (Proportional-Integral-Derivative) control of complex temperature profiles up to 8 ramp/dwell combinations. The maximum temperature allowed is 1300 °C.

This CVD system features a 3-inch diameter growth tube. Figure 2.2 shows the design diagram of the growth tube. It is unique in that the injector is 4-inch inside the main body of the growth tube and end cap is removable for sample loading. The injector is specifically designed for achieving uniform gas flow in the middle of the growth tube. At the taper joint, cap the outer surface of the bulk tube and the inner surface of the end are polished for consistent gas sealing with the temperature ranging from room temperature to higher than 1000 °C. The end cap is mobile to allow easily sample loading. Prior to loading into the process tube, samples are placed on a quartz boat first. After removing the end cap, one can use a loader to push the boat into to the active growth zone. The end cap is then placed back carefully to ensure an airtight seal. The growth tube affords an active growth zone of ~ 2.5” ×6” right in the middle, large enough for regular CNT research.

The major parts and accessories of Nano Furnace are presented in Table 2.1.

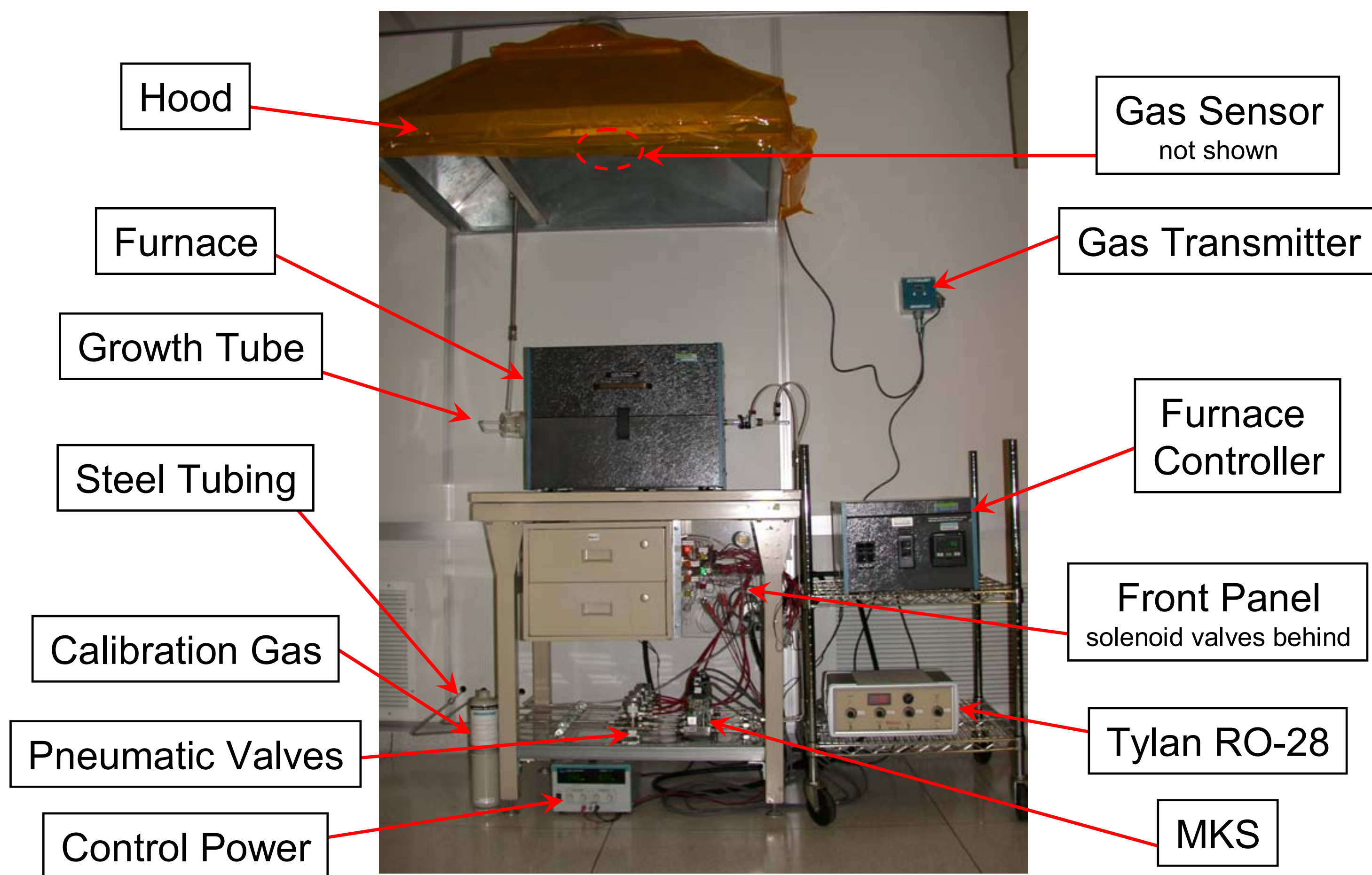

Figure 2.1 A photo of the CVD system.
Gas cylinders (not shown) are stored in the room next to the furnace.

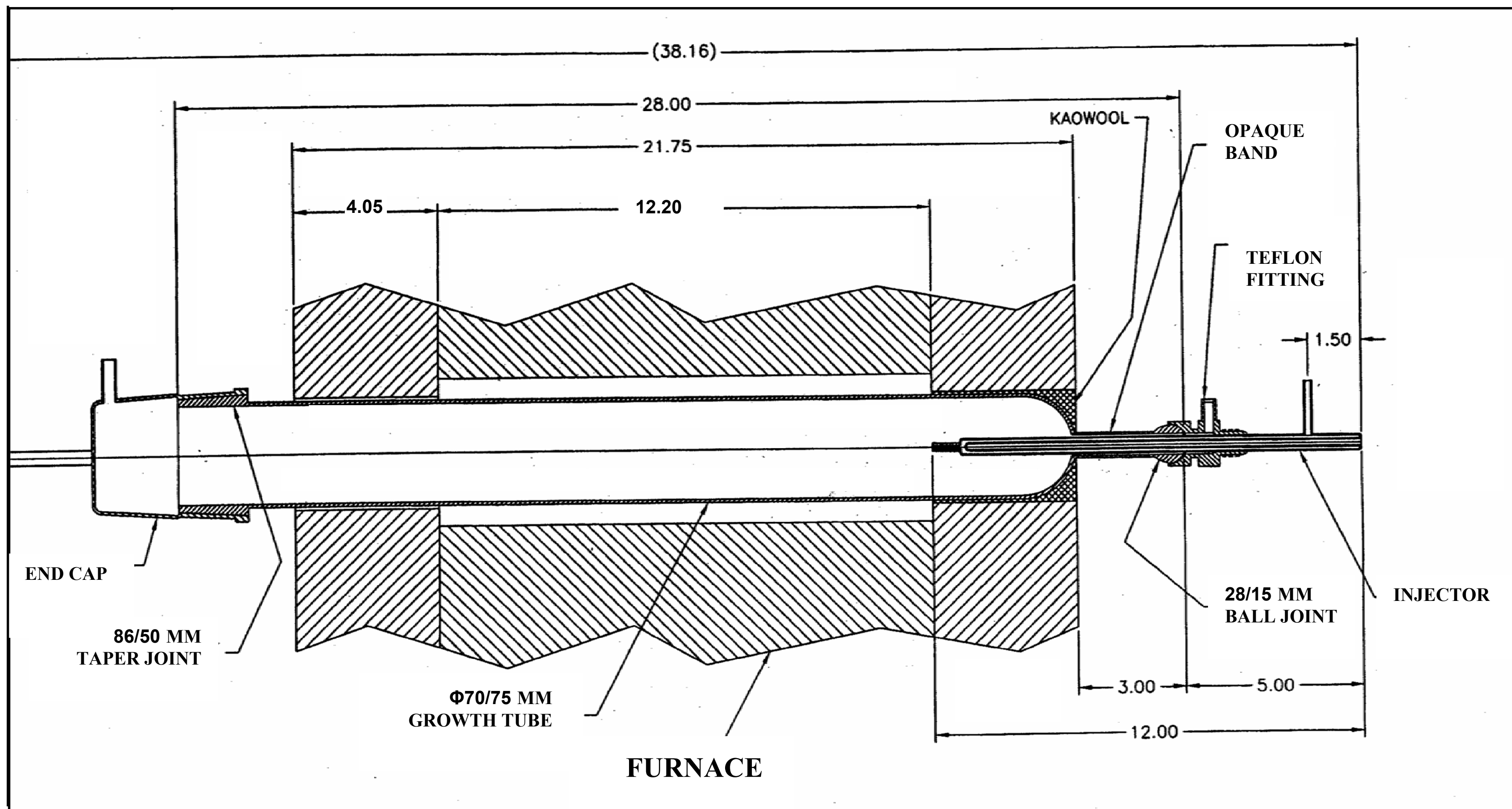

Figure 2.2 Drawing of the growth tube.
(Unit: inch unless specified. Courtesy of Jake Hess)

Table 2.1 Specification of the parts and accessories of Nano Furnace

Part Name	Manufacture	Quantity	Description
Lindberg Furnace	BlueM	1	3-inch
Furnace Controller	Eurotherm	1	Eurotherm 818P Programmer, 120VAC/40A
Process Tube	GM Associates	1	3-inch, Quartz
Injector	GM Associates	1	Quartz
End Cap	GM Associates	1	Quartz
O-Ring Gasket	Swagelok	2	Teflon
Sample Boat	GM Associates	1	Quartz
Sample loader	GM Associates	1	Quartz
Flow Rate Controller	Tylan	1	RO-28
Mass Flow Controller	MKS	5	Calibrated by Coastal Instruments
Pneumatic Valve	Nupro	5	Mechanical valves
Solenoid Valve	Asco	5	3-way, electrical valves
Power Supply	Global Specialties	1	Model 1332A, 0-32 VDC, 0-5 ADC.
Portable Gas Leak Detector	Industrial Scientifi	1	Flammable gas detector
Flammable gas detector	Sensidyne	1	SensiAlert 360
Sensor	Sensidyne	1	Flammable gas sensor
Calibrating gas	Sensidyne	1	Methane 1.5% (30% LEL, mole%) balanced by air

2.1.2 Control System

The gas control system is shown in Figure 2.3. Currently there are five gas inputs for Nano Furnace: nitrogen, argon, hydrogen, methane and ethylene. Among them, hydrogen, methane and ethylene are active gases. Specifically, methane and ethylene work as carbon feedstock and hydrogen is for preventing the deposition of amorphous carbon. Argon is for establishing an inert environment at high temperature (~ 900 °C) before introducing active gases. Nitrogen has three different usages: 1) Nitrogen controlled by pressure gauge PG5 (~ 20 PSI) flows through steel tube into growth tube. It is for maintaining the entire gas passage oxygen free at ambient temperature; 2) Nitrogen gauged by PG6 (~ 80 PSI) flows to steel tubes immediately next to the regulators of cylinders for three active gases. It is solely for safety reason in case purgeing the entire system is needed. MV9, MV10 and MV11 are normally closed. 3) Nitrogen controlled by PG7 (~ 50 PSI) is for actuating 3-way solenoid valves 3W1-3W5. Its importance is going to be described in the later paragraph. Nitrogen is not involved in high temperature process so that its purity is not critical. Nitrogen directly comes from the huge tank that supplies the entire clean room.

Other than nitrogen, all the active gases and argon are at high purity (5N) and are supplied by independent cylinders ordered from Airgas and PraxAir. Gas cylinders are store in a separate room behind Nano Furnace. The pressure of gases (~ 25 PSI for each) flowing toward growth tubes is controlled by pressure gauge PG1-PG4. After flowing through pneumatic valves (MV1-MV4) and mass flow controllers (MKS1-MKS5), all the incoming gases are combined into a single passage. This way reacting gases can be sufficiently mixed along the length of the steel tube before injected into the growth tube.

MKS1-MKS5 are controlled independently via voltages applied by 4 channels of Tylan RO-28. Nitrogen is in use only when the system is standby or when the temperature drops to 100 °C after each growth run. Therefore, it is ok for nitrogen and argon to share Channel 4 of Tylan RO-28 (Please refer to the Nano Furnace Manual in Appendix A).

Because the active gases are flammable and explosive and the temperature is high, typically at 900 °C, considerable care is taken to the safety issue when designing the gas control system. First, the furnace is placed under a hood with negative pressure compared to the environment. All the gaseous exhaust is pumped into the hood, mixed and diluted well below the legal exhaust level by fast flowing nitrogen gas. In addition, a Seni 360 high sensitivity gas sensor is installed right on top of the Lindberg furnace to monitor the gas leakage. A transmitter displays the concentration of flammable gases in real time. Once the concentration of flammable gases reaches the setpoint, the alarm wails and alerts the users to evacuate. The setpoint is 5% LEL, far less than the documented secure exhaust concentration (30 %LEL) for methane and the sensor is calibrated on a monthly basis (as recommended by the manufacture). Furthermore, to minimize the diffusion of the oxygen in the air into the system, pure nitrogen (3N) is flowing constantly through the system when the system is standby, as mentioned in the previous paragraph.

Most importantly, the implementation of a two-valve system (pneumatic valves and solenoid valves) insures the safety in dealing with flammable gases such as hydrocarbon and hydrogen. 3W1-3W5 are 3-way solenoid valves and PVB1-PVB5 are pneumatic valves. When switching solenoid valves, the actuating coils generate a large transient current to counter the suddenly stopped bias current. This transient current is

undesirable and it may induce flash along the circuit. Therefore, solenoid valves are not directly connected to the passage of active gases. Instead, 3-way solenoid valves (3W series in Figure 2.3) are utilized to control pneumatic valves (PV series in Figure 2.4). “Pneumatic” refers to the use of air pressure to operate valves. In our case, the pressure comes from nitrogen gas controlled by a pressure gauge (PG7, 50 PSI).

The ON/OFF of each gas can be explained by using hydrogen as an example. When E3 is closed, solenoid valve 3W3 turns on. Nitrogen flowing from PG7 is applied to pneumatic valve PVB3. PVB3 turns on then hydrogen can flow through. Otherwise, when E3 is open, 3W3 turns off. Nitrogen is released into the environment and thus no pressure is applied to PVB3, which turns off. Then hydrogen is stopped. This process is also listed in Table 2.2. When switching solenoid valves, the actuating coils generate a large transient current to counter the suddenly stopped current. This transient current is very dangerous because it may induce flash along the circuit.

Table 2.2 ON/OFF control of the gas flow in Nano Furnace

Front Panel Switch (E1-E5)	Solenoid Valve (3W1-3W5)	N_2 Pressure (from PG7)	Pneumatic Valve (PVB1-PVB5)	Target Gas
ON	ON	Applied	ON	ON
OFF	OFF	Released	OFF	OFF

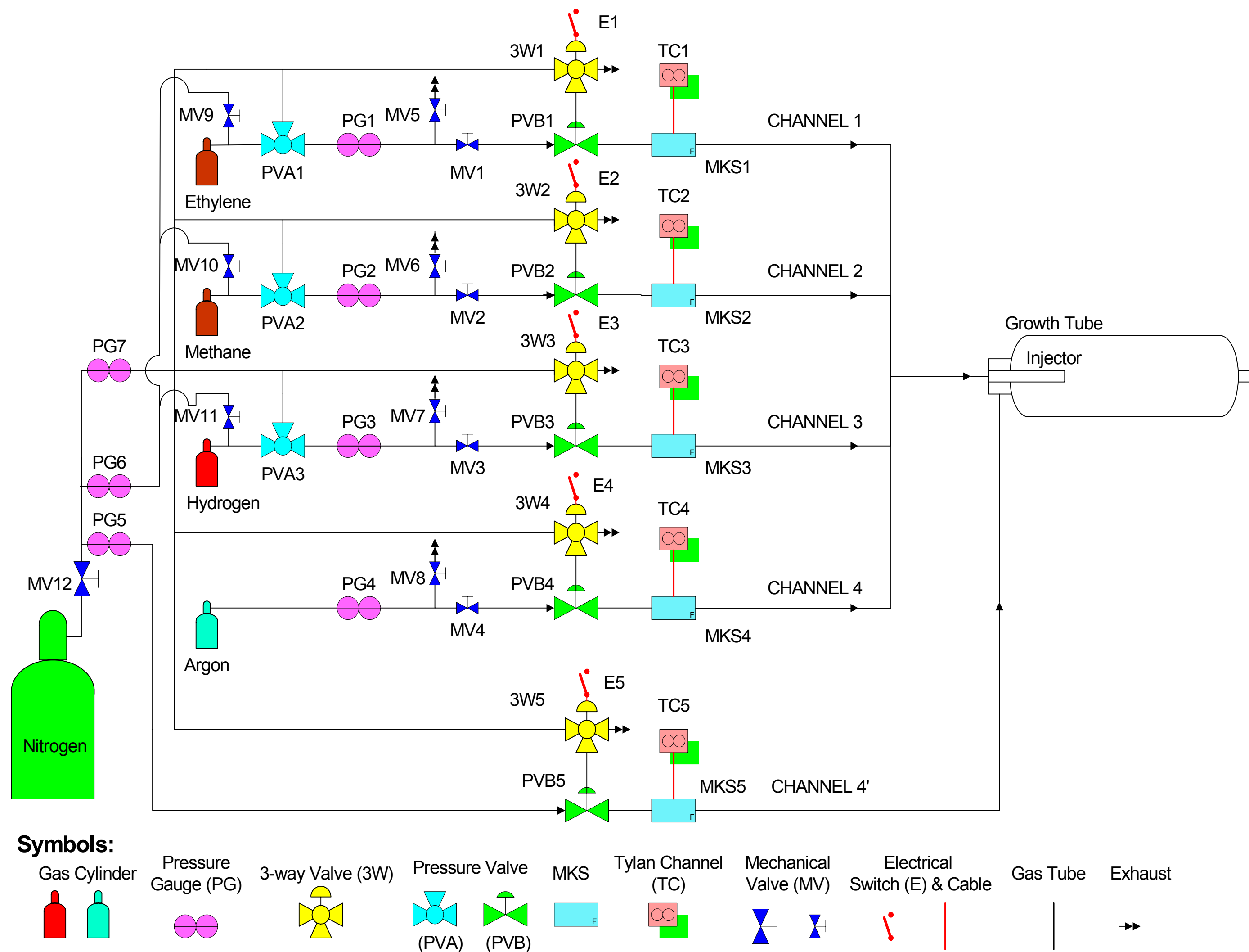

Figure 2.3 Design diagram of the gas control system.

Table 2.3 Specification of the gases.

Gas	Purity	Vendor	Cylinder Volume	Initial Pressure (PSI)
Nitrogen	3N	Airgas	N/A*	120**
Argon	5N	PraxAir	40 CFT	2000
Hydrogen	5N	PraxAir	40 CFT	2000
Methane	5N	PraxAir	3.5 CFT	2000
Ethylene	5N	PraxAir	3.5 CFT	2000

(CFT: Cubic Feet. *: N2 is from the huge that that supplies the entire clean room. ** 120 PSI is the pressure of nitrogen for general purpose in INRF, not the pressure of the nitrogen tank.)

The control circuit of Nano Furnace is very simple, as shown in Figure 2.4. Note that a diode is connected in parallel with each solenoid valve to short the likely transient current mentioned previously.

Nano Furnace is currently under manual control. However, both Eurotherm 818P and Tylan RO-28 have serial port (e.g. RS232) and Nano Furnace can be integrated with a software interface to enable computerized control. The design of Nano Furnace affords very good CNT growth that will be discussed extensively in the following chapters.

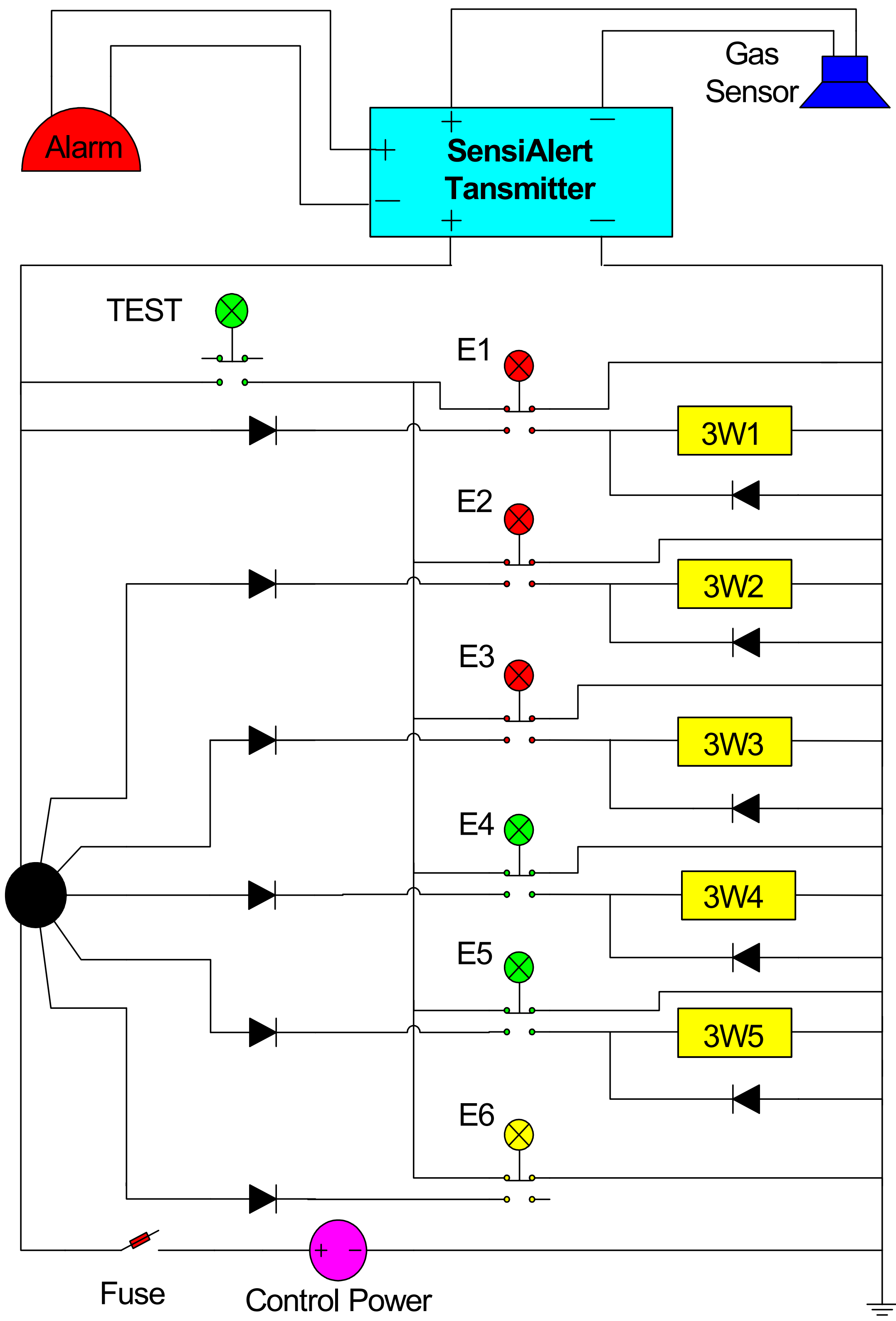

Figure 2.4 Circuit diagram for the control electronics.

2.2 Catalyzed Growth of Carbon Nanotubes on Nanoparticle Catalyst

2.2.1 Introduction

Patterned growth of single-walled CNTs based on a combination of oxide nanoparticles and transition metal catalyst has been developed by Kong et al. in 1998 [6]. The nanoparticles are deposited onto a substrate with lithographically defined wells after spinning on a nanoparticle laden solution, followed by a drying step and then lift-off. There, alumina nanoparticles combined with transition metals are typically mixed and dispersed in organic solvents such as methanol and then spun onto a wafer with pre-patterned PMMA wells. This requires either 1) electron beam or deep UV lithography to pattern PMMA directly, or 2) a multi step process involving patterning both PMMA and photoresist (Methanol cannot be spun onto wells patterned into photoresist directly because it attacks the photoresist). We have developed a simplified method for patterning oxide nanoparticle and transition metal catalysts using water as the solvent.

2.2.2 Aqueous Catalyst Recipe

Using conventional photolithography we fabricated wells directly in photoresist (Shipley 1827) on the silicon (or quartz) substrate. Next, 2.0 g of alumina nanoparticles (Degussa, aluminum oxide C), 2.5 mmol $Fe(NO_3)_3 \bullet 9H_2O$ (Aldrich), and 0.7mmol $MoO_2(acac)_2$ (Aldrich) were added to 60 ml DI water in sequence while stirring violently. Since $Fe(NO_3)_3$ is soluble in water, spinning its solution directly onto the wafer would

leave little Fe. This would be an undesirable consequence, essentially throwing out the baby with the bathwater, since the Fe plays a crucial catalytic role in the nanotube growth. To alleviate this problem, 15 ml of ammonia (concentrate) was slowly dropped into the mixture above. This caused the formation of $Fe(OH)_3$, which precipitates:

$$NH_3 + H_2O \leftrightarrow NH_4^+ + OH^-$$

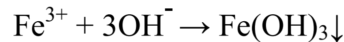

$$Fe^{3+} + 3OH^- \rightarrow Fe(OH)_3\downarrow$$

The mixture was stirred for 24 hours followed by sonication for 3 hours, resulting in a suspension of 1.25 mmol Fe_2O_3/0.7mmol MoO_3/2.0 g alumina and water. Two drops of this mixture were deposited onto samples patterned with photoresist (Shipley 1827) using photolithography. After spinning at 3400 rpm for 40 seconds, and after a 100 ˚C, 20 minute bake, lift-off of the photoresist in acetone and methonal led to the final sample with catalyst pattern ready to carry out CVD. This process is shown in Figure 2.5.

Shipley 1827 after development was very robust with respect to the catalyst mixture, which allowed well-defined catalyst pattern at least to the micrometer scale. One more advantage of our aqueous catalyst recipe is that no toxic chemical such as hydroxylamine [25] is involved.

This work was presented to the 3rd IEEE Conference on Nanotechnology, San Francisco, 2003 [26].

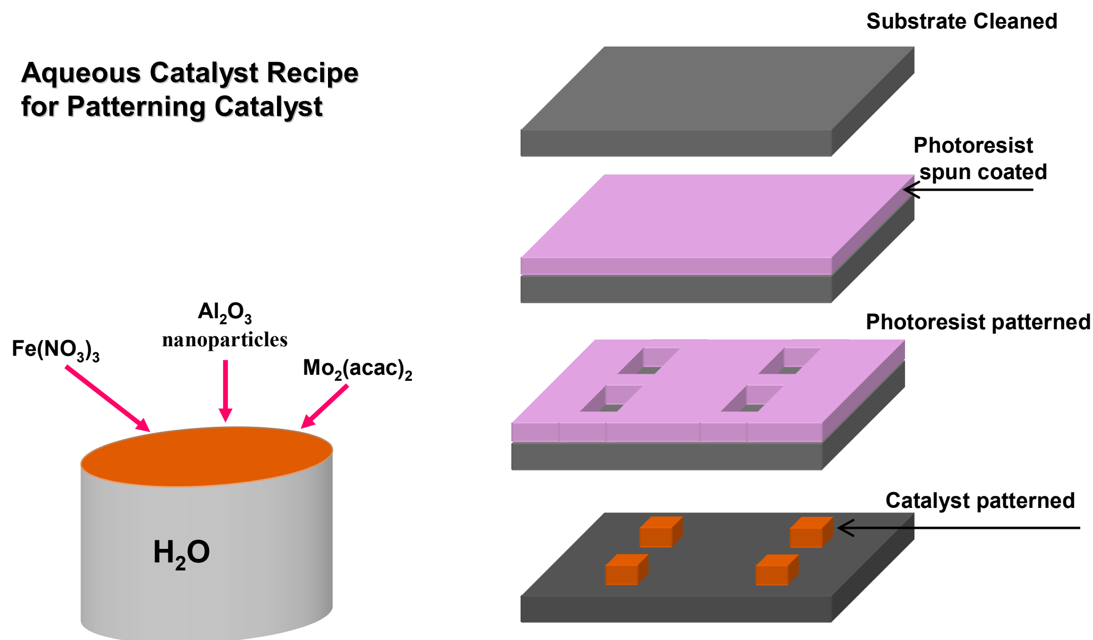

Figure 2.5 Process of patterning aqueous catalyst

2.2.3 CNT Growth

Referring to various references on the catalyzed growth of CNTs using nanoparticle catalyst, we successfully developed a manual for the growth of CNTs using our Nano Furnace. The manual is enclosed in Appendix A. A typical growth run is as follows:

1) Load sample.

Prior to loading into the process tube, samples are placed on a quartz boat first. After removing the end cap, one can use a loader to push the boat right into to the active growth zone. The end cap is then replaced carefully to ensure an airtight seal. Schematic depiction of the samples inside the process tube is shown in Figure 2.6.

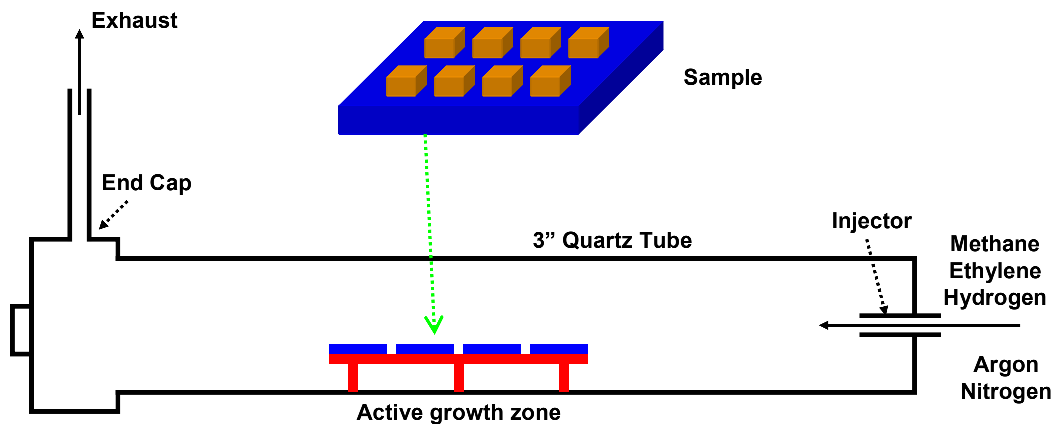

Figure 2.6 Schematic depiction of CNT growth.

2) Grow Carbon Nanotubes

CVD started with heating up the quartz tube to 900 °C under a constant argon flow. The argon was replaced by a co-flow of 1000 sccm CH_4 (99.999%) and 200 sccm H_2 for 10 to 15 minutes after the temperature was stable at the setpoint. At the final stage of the active growth, temperature started to drop, as programmed by Eurotherm 818P. The methane was shut down first, argon was turned on and then hydrogen was turned off. It took several hours for the growth tube to cool down naturally to room temperature in the air. During this period of time, argon was constantly flowing through the quartz tube to maintain an inert atmosphere inside the process tube. We typically grew CNTs on individual 1” × 1.5” chips, the effective growth zone of 2.5” ×6” allowed appreciable parallel processing capability. Representative gas profile and temperature profile is shown in Figure 2.7 and Figure 2.8, respectively.

3) Unload samples

Samples can be securely unloaded from Nano Furnace when the temperature of the growth tube drops to less than 100 °C. In control experiment, samples patterned with the same catalyst and experience the standard CVD growth sequence were taken out from the process tube at 300 °C. No CNTs were observed. The reason is that CNTs were instantly burned in the air once in contact with the oxygen. CNTs are subject to doping and oxidation at relatively ambient temperature. This hinted us to go beyond oxide to find an appropriate dielectric for gating CNTs, which is discussed in detail in Chapter 3.

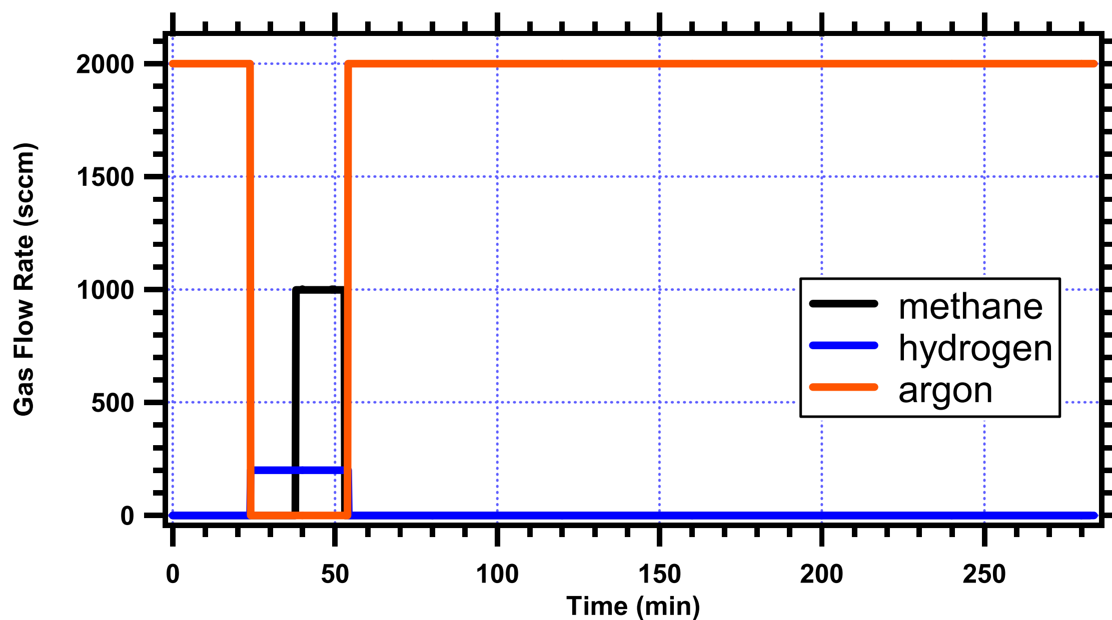

Figure 2.7 A representative gas profile

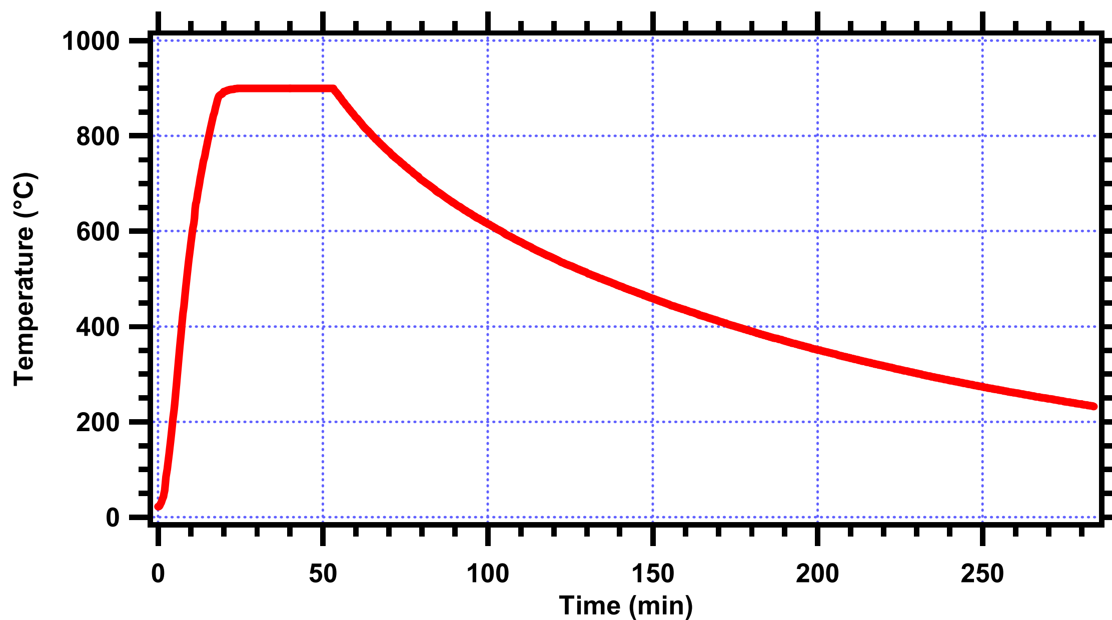

Figure 2.8 A representative temperature profile

2.2.4 Growth Results and Discussion

The most important process parameters that affect the outcome of CVD growth are the temperature and flow rates. In general the high temperature allows the maximal thermal annealing and thus prevents the formation of any structural defects on the CNTs. In our case, we find that temperature higher than 950 °C tends to promote the thermal pyrolysis of hydrocarbon gases into amorphous carbon. When the temperature was set at 1000 °C, we observed back soot deposited on the wall of the quartz tube. Probing the surface of an oxidized silicon wafer experienced the CVD, significant conduction was measured everywhere. This leads us to infer that there is significant deposition of amorphous carbon at 1000 °C. With respect to carbon feedstock, we specifically select methane because it is the most stable hydrocarbon gas and its self-decomposition is minimal. The high thermal stability of methane and the typical growth temperature of 900 °C create an environment where the methane is reactive and decomposable only on the catalyst (Fe/Mo/alumina). Our control experiment also show that there is no decomposition of methane at 900 °C without the presence of the catalyst, thus verifying the growth of CNTs in our case is indeed a catalyzed process.

The flow rate and flowing time of hydrogen is also critical to the growth of single-walled CNTs. First, hydrogen at elevated temperature prior to introducing methane can reduce iron oxide to form very reactive elementary iron, which may be the real catalyst that affords the growth of single-walled CNTs. Second, co-flowing hydrogen with methane during the active growth suppress the self-pyrolysis of the later gas, which tends to form undesirable amorphous carbon. On the other hand, the hydrogen flow rate shouldn't be too high compared to that of the methane because ultrahigh hydrogen

concentration in the process tube can completely suppress the formation of CNTs. At the end of the active growth, hydrogen should be turned off right after turning off methane. CNTs can be completely etched away by hydrogen at elevated temperature. We had even specifically replaced two samples with CVD grown CNTs into the process tube. The same CVD growth run was carried out following the manual except introducing methane. SEM images post growth demonstrated that all the old CNTs were gone. This may be useful when a process of etching or shortening CNTs is desired. Interestingly, hydrogen not only etches CNTs but also clean away amorphous carbon. The black fume accumulated on the wall of the process tube can be cleaned all the way by flowing hydrogen for a certain period of time at > 800 °C.

Samples after CVD were characterized by SEM and AFM extensively. In general, AFM is used to measure the diameter of CNTs because of its atomic scale resolution and SEM is more convenient in measuring the length, orientation and location of CNTs.

A. AFM Characterization and Discussion

An AFM (Digital Instruments, Multimode) working at tapping mode was used to image our samples. In this mode the tip extends into the repulsive regime (but not in direct contact) of the surface so the tip intermittently taps the surface. The cantilever spring oscillates at its resonance frequency, which is influenced by forces applied by the sample. The frequency deviation is used to make a topographical image, or height image, of the sample. Tapping mode is advantageous in improving the lateral resolution and reducing damage to the samples. In addition, the AFM simultaneously generates a phase contrast image. In phase mode imaging, the phase shift of the oscillating cantilever

relative to the driving signal is measured and analyzed to reflect the surface inhomogeneity. Height image is usually adopted to characterize CNTs.

The diameter of CNTs as-obtained is less than 4 nm (typically ~ 1.5 nm), which is consistent with previous data of single-walled CNTs obtained under similar growth conditions [6]. Thus we infer they are also single-walled. Two representative AFM images are shown in Figure 2.9. Figure 2.9 (a) shows a CNT 3.2 nm in diameter. The diameter of CNTs in Figure 2.9 (b) is no greater than 1.5 nm, which is typical of as-grown carbon nanotubes.

While the spatial resolution of AFM is very high, its speed is severely limited by the serial nature of its probing tip and the slow speed of the current mechanical scanner. Massive and time efficient imaging of CNTs in this work is presumably carried out using SEM.

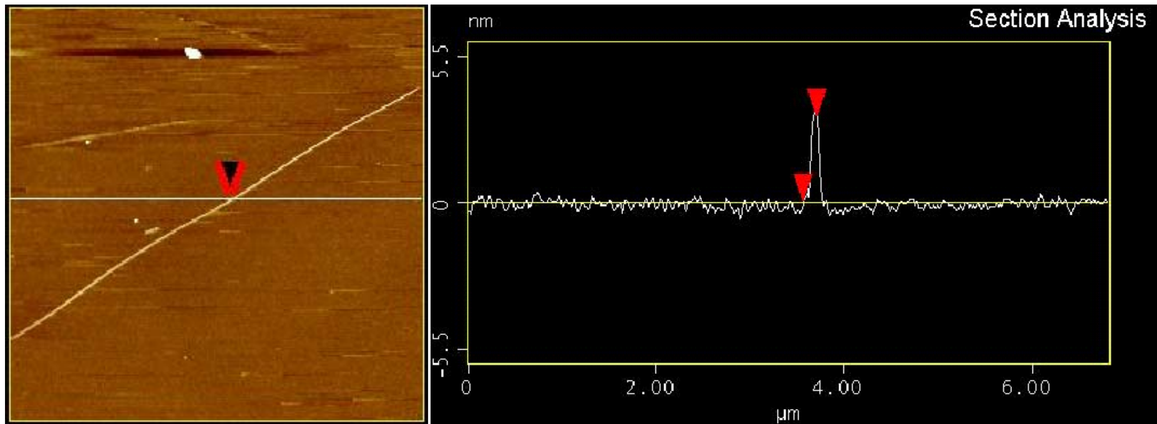

(a) AFM image of a carbon nanotube (3.2nm).

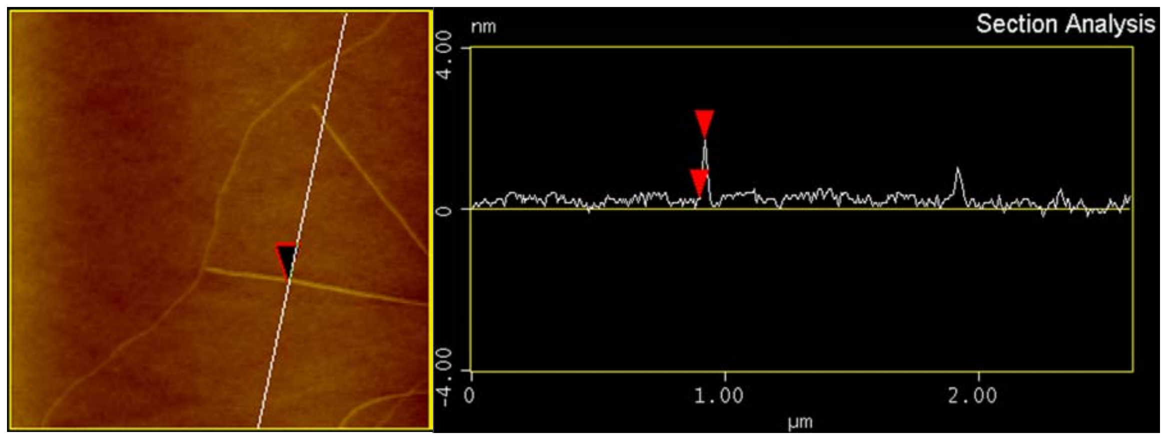

(b) AFM image of a CNT1.5nm in diameter. The diameter of the other two is less than 1 nm.

Figure 2.9 AFM images of CNTs grown on nanoparticle catalyst. (Height image)

B. SEM Characterization and Discussion

A Hitachi S-4700 SEM is utilized to characterize our samples. In SEM, electrons are liberated from a field emission source and accelerated in a high electrical field gradient. Within the high vacuum column the so-called primary electrons are focused and deflected by electronic lenses to produce a narrow scan beam that bombards the object. As a result, secondary electrons are emitted from each spot on the object. The angle and velocity of these secondary electrons reflects the surface structure of the object. A detector catches the secondary electrons and produces an electronic signal. This signal is amplified and transformed to a digital image that is displayed on a monitor in real time, which can also be saved and processed further.

In our case, SEM has to deal with CNTs on insulating substrate such as silicon wafer with thick SiO_2 and quartz wafer. Insulating substrate such as SiO_2 is charged negatively when scanned by the electron beam. Differences in surface electrostatic potential affect the number of secondary electrons emitted from SiO_2. Namely, a positive surface potential will increase the number of secondary electrons, while a negative surface potential will decrease the number of secondary electrons. Specifically, the bright contrast is due to increased secondary electron emission from the SiO_2 arising from positive surface potential relative to the SiO_2 bulk; and the dark contrast is due to decreased secondary electron emission from the SiO_2 arising from negative surface potential relative to the SiO_2 bulk. The voltage contrast mechanism of imaging of CNTs on insulating surface using SEM is discussed in detail in reference [27].

The typical acceleration voltage was 1 KV. Higher acceleration voltage usually gives rise to serious charging of the substrate and thus distorted or even disables the

imaging process. In addition, the low acceleration minimizes the possibility of electron beam damage of the CNTs.

The nanoparticle catalyst produced CNTs in abundance in the vicinity of catalyst sites. The absence of CNTs isolated from catalyst sites suggests that nanoparticle catalyst played a critical role in the CVD process, where CNTs grew by catalyzed decomposition of hydrocarbon gases rather than the self-pyrolysis. Self-pyrolysis of hydrocarbon gases generally yields a high percentage of amorphous carbon. Preventing the deposition of amorphous carbon is of paramount importance in fabricating working CNT electronic circuits in that unwanted amorphous carbon can cause short circuits.

A majority of CNTs emanating from the catalyst sites take a U turn back to the catalyst site. However, there are always CNTs making their way all the way away from the catalyst sites as shown in Figure 2.10. The marked CNT is ~ 320 μm in length. This CNT is very curly at the micrometer scale; however, sharp kinks at atomic scale are not seen when zoom-in. Occasionally, CNTs fold into a circle as shown in Figure 2.11. There are also very straight and long CNTs grown from the same catalyst pads under the same growth conditions. The marked CNT in Figure 2.12 is a good example. It is smooth within the entire length of ~ 80 μm. There are typically 5 to 10 CNTs as such in a quarter of 4-inch wafer. This kind of CNTs may have fewer defects in longer range than those curly ones. These CNTs emanating far away from the catalyst sites are of special importance for this thesis research. Because of the extraordinary length, I am able to align metal leads to these CNTs using a self-marked process that is discussed in detail in Chapter 3.

Figure 2.10 A CNT 320 μm in length.
(Scale Bar: 50 μm)

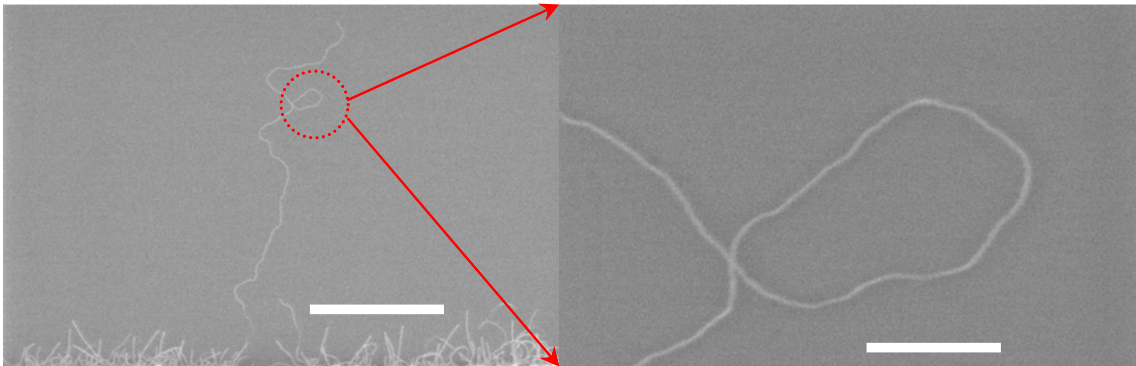

Figure 2.11 A CNT with a buckle.
Left scale bar: 30 μm, right scale bar: 3 μm.

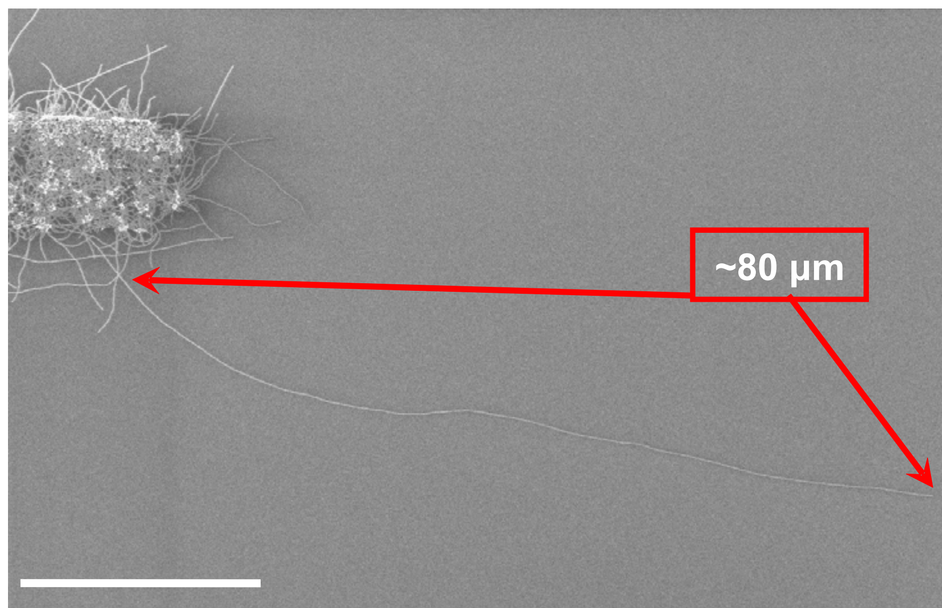

Figure 2.12 A smooth CNT 80 μm in length.
Scale bar: 30 μm.

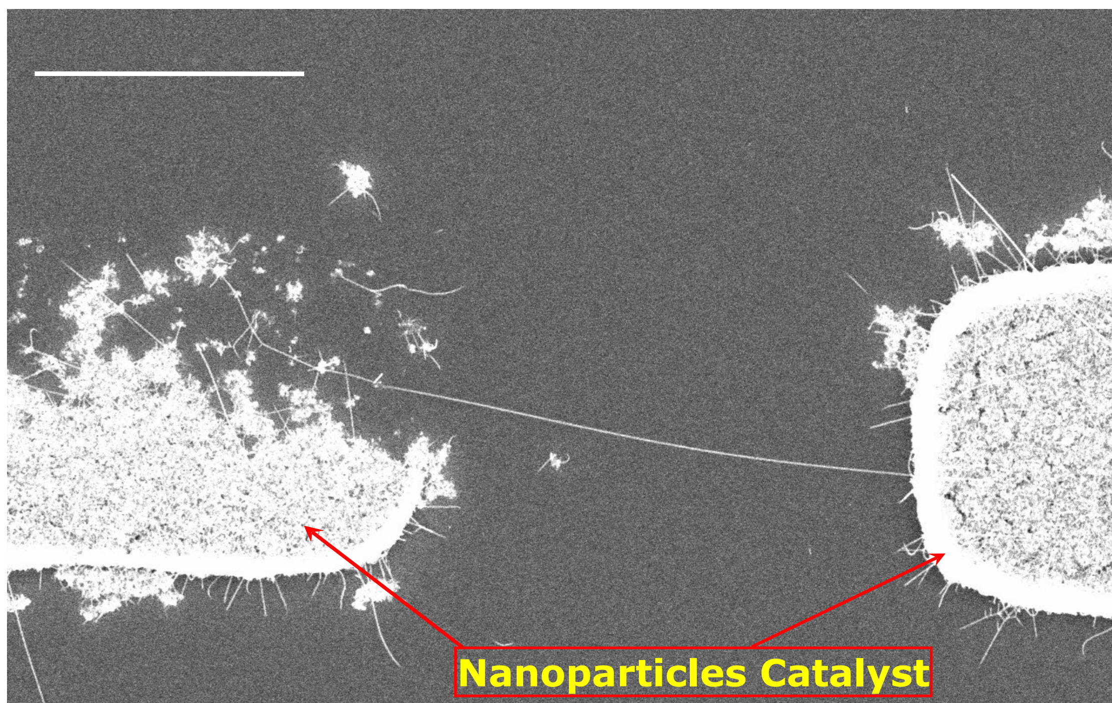

Figure 2.13 A CNT bridging a pair of catalyst pattern.
Scale bar: 10 μm.

In general, the growth of CNT will terminate upon touching another catalyst site. This hints us to control the length of CNTs by using catalyst pairs with predefined gaps. In Figure 2.13, we show a CNT bridging a gap of 16 μm. The control of CNTs is also very important when it comes to device applications. However, our progress toward this aim is still limited. Typically, there are more than one CNT bridging the catalyst gap.

These figures also reveal the common feature for the nanoparticle catalyst pattern itself. First, nanoparticle catalyst pattern can be defined precisely to the micrometer scale. In addition, catalyst pattern is not flat and uniform in general. In some region where the catalyst is suppose to be present, nanoparticles completely disappeared during lift-off. Although both disadvantages can be minimized using more dilute catalyst solution and finer catalyst feature, the solution based patterning approach is not precise sufficient for make integrated circuits at nanometer scale. In the next section we will present our progress using metal thin catalyst.

To investigate the electrical properties of CNTs at high frequencies, we also patterned nanoparticle catalyst on high resistivity silicon wafers and quartz wafers to grow CNTs. The growth result is very similar to those on the oxidized Si wafers.

2.3 Catalytic Growth of Carbon nanotubes on Metal Thin Film Catalyst

2.3.1 Motivation

While our aqueous catalyst recipe simplified the lithographical process involved in catalyst patterning, it is still subject to the limitation of wet chemical processing, which are time consuming and difficult to use for patterning nanoscale features. An alternative approach would be to directly evaporate the metal thin film catalyst onto a wafer, as is commonly done in the semiconductor industry, using either electron beam evaporation, thermal evaporation, or sputtering techniques.

Thin film based catalysts could have many advantages over solution based, spun-on catalyst: First, it is quick, easy, precise and amenable to produce small patterns. Second, it is more compatible with well-established processes used in the semiconductor industry. Third, it is potentially more reliable and reproducible. Fourth, it is in principle compatible with electrical contacts to nanotube ends. The as-grown CNTs may already be electrically in contact with the remnants of the thin metal film. (In contrast, the growth from insulating catalysts seems less compatible with electrical contacts at the microscopic level.) Fifth, by using ferromagnetic metals such as Co as the catalysts, these electrical contacts could be used to inject spin-polarized electrons directly into the nanotubes for applications in nano-spintronics. Sixth, the technique is scalable, crucial for future massively parallel nanotube integrated circuits.

Our progress towards our goal of developing a process to grow high quality SWNTs with CVD between lithographically patterned thin metal film catalyst sites is presented in the following sections.

2.3.2 Catalyst Patterning and CVD

Wafers with lithographically patterned photoresist were loaded into the chamber of an electron beam evaporator, metal thin films were then evaporated by electron beam heating of the targets. The deposition rate can be controlled by adjusting the beam current. We prepared Ni thin film of different thickness to investigate the dependence of the nature of CNTs on metal catalyst.

CVD was carried out using our Nano Furnace and also EasyTube (FirstNano, Inc. Santa Barbara, CA), which is similar to Nano Furnace but features a 1.5 in growth tube. The gas temperature profile is similar to that in Section 2.2. And sometimes, to directly compare the growth result of nanoparticle catalyst and thin metal film catalyst, they were placed next to each other in the in growth tube.

2.3.3 Growth Results and Discussion

For the growth result from our Nano Furnace, Ni thin film catalyst generally resulted in short and large diameter MWNTs. A SEM image of a typical growth result from EasyTube is show in Figure 2.14. The diameter of the nanotubes grown with nickel catalyst varied between 10 and 40 nm as measured under the SEM, which is much larger than the measured diameters of the nanotubes grown with the nanoparticle catalyst. TEM

analysis revealed these to be MWNTs, as shown in Figure 2.15. And we also notice that samples with nanoparticle catalyst experienced the same growth run resulted in single-walled CNTs. We speculate that this may be due to the thickness of the Ni catalyst. The process of CNT growth by catalytic CVD can be simply described as: the catalyst/nucleation particles dissociate the molecules of the carbon feedstock and then collect the carbon and organize it into a nanotube. CVD Catalyst particles/nucleation centers determine the diameter of CNTs [2]. When the sample was heated up to 900 °C, the metal thin film agglomerated to form metal droplets on the silicon wafer. And the apparent size of these droplets should be no less than 10 nm, which then determined the diameter of those CNTs grown. In the case of nanoparticle catalyst, iron oxide is impregnated in and bulk alumina scaffold, which has very large surface areas and remains stable at more than 1000 °C. Alumina keeps the metal particles from aggregating into larger particles at high temperature, and thus amorphous carbon and fiber are prevented. Detailed mechanism of CNT growth is beyond the scope of this thesis and can be found in reference [2].

While single-walled CNTs or small diameter CNTs were reported to grow from Fe-Ni [28] and Ni/Al thin films, we have not achieved this aim yet. The reason may lie in: 1) different technology used in depositing thin metal film; 2) different growth conditions. Using metal thin film to grow SWNTs would represent a significant simplification in SWNTs growth compared to the nanoparticle method which requires preparing, spinning casting and drying nanoparticle laden catalyst solution. We are still working towards growing high quality SWNTs on thin metal films.

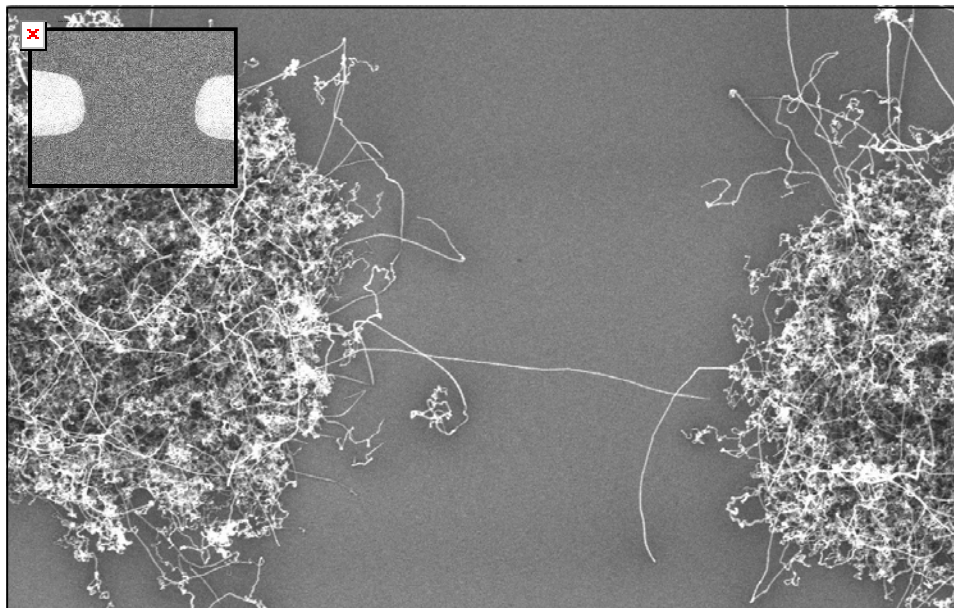

Figure 2.14 SEM image of CNTs grown from Ni thin film catalyst.

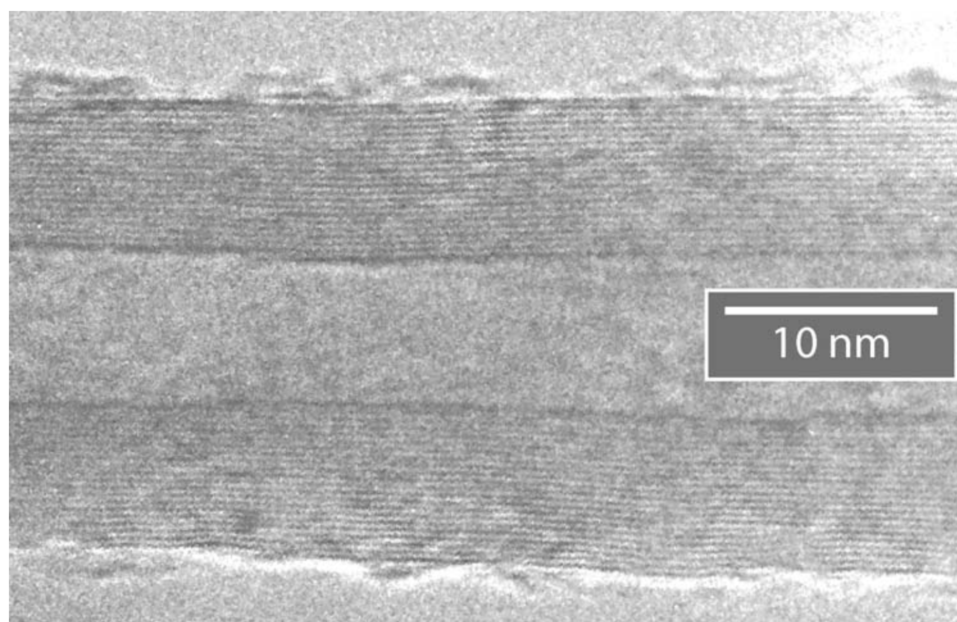

Figure 2.15 TEM image of nanotubes grown from nickel thin film catalyst.

2.4 Summary and Perspective

We have successfully developed a chemical vapor deposition system for the growth of CNTs. The 3” tube affords appreciable scalability and the control module enables easy and safe control of the growth parameters. While the precision of nanoparticle catalyst pattern need to be further improved, our aqueous catalyst recipe is more adaptable than the organic counterparts. Combined with Nano Furnace, the aqueous catalyst repcipe affords ultra long single-walled CNTs, which is not trivial when it comes to device applications and, in particular, the electrical properties of CNTs at high frequencies [26]. The reliability of Nano Furnace and the reproducibility of the aqueous catalyst recipe are attained by more than 50 growth runs and ~ 300 independent samples till the end of 2003. Future work is focusing on controlling the nature of CNTs in terms of length, location, orientation and more challenging, chirality.

CHAPTER 3

TOP-GATED CARBON NANOTUBE FIELD EFFECT TRANSISTOR

While the remarkable properties of CNTs make them very promising candidates for electronic applications, a challenging task is to integrate complex arrays of CNTs into electronic devices and circuits. To date, precise control of the length, orientation and location of CNTs is still a hot topic of research. Electron beam lithography, which moves a small electron beam spot with respect to the wafer to expose the wafer one pixel at a time, offers great flexibility in aligning submicron random structures such as nanowires and nanotubes. However, the throughput of electron beam lithography is very limited. An alternative approach is to grow CNTs from catalyst pads patterned by photolithography to improve controlling of the nature of CNTs. This way, it is possible to use conventional optical aligners to address individual CNTs. Indeed, all the devices discussed in this thesis are fabricated using two optical aligners: Quintel Model 2100 and Karl Suss MJB3.

In the first section, I present a self-marked process to align CNTs using conventional photolithography. Next, CNTs prepared by CVD are integrated into electrical devices. The fabrication and characterization of top-gated CNT field effect transistors using silicon nitride as gate dielectric is demonstrated.

3.1 Self-marked Photolithography

The first challenge of aligning individual CNTs is the invisibility of CNTs under optical microscope. The available equipments typically used in identifying CNTs are AFM and SEM. The characteristics of both microscopes are discussed in Section 2.2.4. SEM offers appreciable advantage over AFM with respect to imaging speed. SEM also provides sufficient information about the location, orientation and length of CNTs, at least at the micrometer scale, matching the resolution of our available photolithography systems. The process of electrically contacting individual CNTs is as follows:

1) Catalyst sites are precisely defined as discussed in Chapter 2 prior to CVD growth. Catalyst pattern has to be thick enough to be visible after coating photoresist under optical microscope.

2) After CVD, SEM is used to coordinate the "significant[*]" CNTs with respect to catalyst pattern. The location, orientation and length of CNTs are simultaneously marked on the map of catalyst pattern.

3) "Significant" CNTs are then aligned to electrode pattern under optical microscope according to the map generated in Step 2.

4) Metallization is carried out using an electron beam evaporator and lift off result in CNTs contacted by metal, typically Ti and Au double layer.

In this process, catalyst patterns not only catalyze the growth of CNTs but also work as markers in aligning CNTs. No additional lithography step is needed to put down

[*] "Significant" means the particular individual CNT is reasonably far away from the others and can be individually aligned using Quintel 2100 or Karl Suss MJB3. The 80 μm long CNT shown in Figure 2.12 is a good example.

markers after CVD, as commonly done in electron beam lithography. Thus we name this process as self-marked photolithography in the sense existing features on the wafer are used to provide in-situ markers without adding any additional lithography steps and no electron beam lithography is involved. An example of an individual CNT is successfully contacted by metal electrode is shown in Figure 3.1 (a). These two electrodes can work as drain and source for electrical measurement. A third terminal can be added to the device using the substrate as back gate. Additionally, top-gate can also be fabricated by further processing. The detailed process is described in Section 3.2.

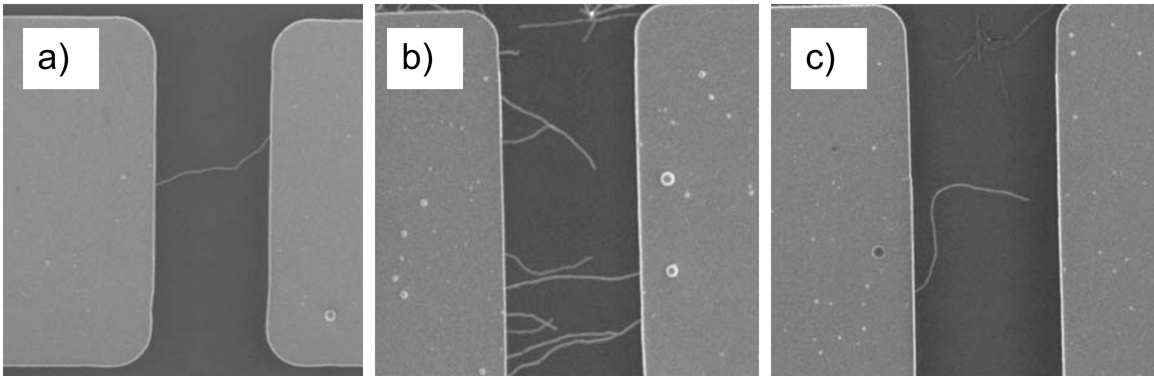

Figure 3.1 CNTs contacted using self-marked photolithography.
(a) An individual CNT between two electrodes; (b) More than one CNT are contacted; (c) A CNT is not fully contacted. All the three samples are aligned using the same electrode mask and undergo the same metallization step (Au (100 nm) / Ti (10 nm)). The gap between two electrodes is the same: 10 μm.

Step 3 is the most critical and challenging step in reality. And it typically takes hours to successfully align an individual "significant" CNT. Sometimes, more than one CNT is contacted, as shown in Figure 3.1 (b). It happens because electrode pattern is so broad that neighboring CNTs are also contacted. The electrode pattern on optical mask is fixed and gives rise to most of the problem. In this sense, electron beam writer is a lot more flexible than optical aligners in dealing with "random" structures such as CNTs.

Another common problem in this process is missing to contact one end of a CNT as shown in Figure 3.1 (c). To minimize this kind of problems, we have to be very selective in choosing "significant" CNTs. As a result, we have to discard a great many very high quality CNTs just because they are too close to the others. Therefore, the throughput is also limited. During the course of this thesis research, 30 devices with only one CNT and more than 150 devices with multiple CNTs have been made this way.

Future work will focus on growing CNTs in a more organized manner. Assembling CNTs into electronic circuits using electrical fields [29], micro fluid [30] and/or chemical/biological functionalization [31] will be a very interesting research topic.

3.2 Top-gated CNTFET using silicon nitride as gate dielectric

3.2.1 Introduction

In terms of gating CNTs, the most widely used gate structure has been macroscopic, doped Si substrate as back-gates and thermally grown SiO_2 [32] or native Al_2O_3 [18] as gated dielectric. As a result, high gate voltages are required to switch the devices on. In addition, use of the substrate as a gate implies that all devices are turned on and off simultaneously, precluding operation of all but the most simplistic circuits. Furthermore, CNTs in all the back-gate design are exposed to the environment, which leads to uncertainty that CNTs may be chemically doped by species in surroundings. Recently, an electrolyte solution has been used to gate CNTs to achieve improved performance [15]. While scientifically interesting, the technologically relevance of this approach is limited.

Of the various geometries for carbon nanotube field effect transistors (CNTFETs), top-gated CNTFETs (as shown in Figure 3.1) are the most promising because they allow local gate biasing at low voltage, high speed switching and high density of integration. To date, two kinds of oxide thin films have been developed as gate dielectrics for CNTFETs: the first method uses low temperature oxidation (LTO) to deposit SiO_2 thin film from SiH_4 and O_2 at 300°C [33]; the other method implements atomic layer deposition (ALD) to deposit ZrO_2 from $ZrCl_4$ precursor and H_2O oxidizer in a N_2 carrier gas [34]. Although both processes have resulted in CNT transistors with conventional MOSFET like I-V

characteristics, whether these experiments have really revealed the intrinsic properties of CNTs is under scrutiny in that a significant defect density to the CNTs may have been introduced by their oxygen associated reactants. It is known that CNTs are prone to oxygen doping at room temperature [35] or at least oxygen changes the metal/CNT contact [36]. And in our experiments we also found out that CNTs could be burned in air at > 300 °C. Therefore, an appropriate gate dielectric involving a completely oxygen free environment should be more chemically benign to CNTs in the first place and allow the investigation and application of the superb intrinsic properties of CNTs.

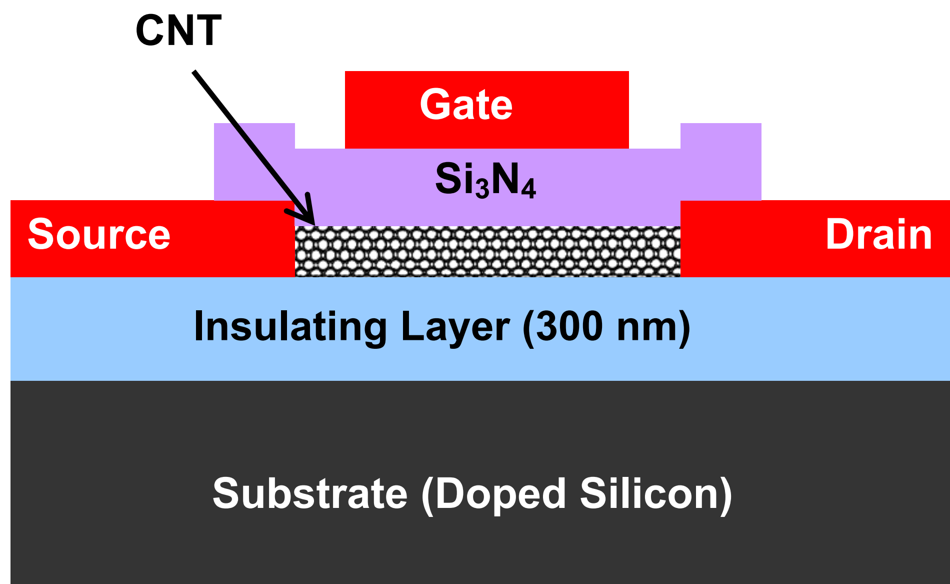

Figure 3.2 Schematic cross section view of top-gated CNT transistor

3.2.2 Why Silicon Nitride

Silicon nitride has been intensively investigated for decades as an alternative to SiO_2 gate dielectric due to its relatively higher dielectric constant (κ = 7.8) [37], strong

resistance to impurity diffusion and compatibility with conventional CMOS processes. Numerous attempts to develop the CVD silicon nitride into a viable gate dielectric directly for CMOS have encountered two principal difficulties: (1) poor nitride/Si interface properties and (2) high density of bulk traps in silicon nitride. The first difficulty does not apply to CNTFETs, where CNTs are usually placed on either thermal silicon dioxide or quartz and silicon nitride is in direct contact with silicon dioxide rather than the silicon body. The nitride/oxide stack dielectrics have shown promising results for continued downscaling of CMOS devices [38], [39]. The other downside is far more complicated and emerging thin film deposition techniques such as ALD [40] and jet vapor deposition (JVD) [37] have shown very encouraging results.

Most importantly, the advantage of silicon nitride over oxide as gate dielectric for CNTFETs lies in the chemical process that is benign to CNTs. Silicon nitride thin film is usually deposited from a mixture of reactant gases of SiH_4 and N_2 or NH_3. Film formation takes place as a result of reactions between a number of excited species such as excited molecules of NH_3 (or N_2) and SiH_4, NH, NH_2 (radicals), and unexcited molecules and their condensation on the substrate [41]. The overall reaction is:

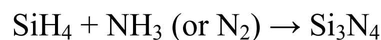

$$SiH_4 + NH_3 \text{ (or } N_2) \rightarrow Si_3N_4$$

Oxygen associated species are absent from the Si_3N_4 deposition process and ammonia and its derivatives should be more benign to CNTs as shown in [42] , where NH_3 excited by plasma is found to play a crucial catalytic role to promote the growth of CNTs.

3.2.3 Device Fabrication

3.2.3.1 CNT Growth

The CNTs were grown from lithographically patterned nanoparticle catalyst sites using CVD [6]. The nanotube growth procedure and recipes are described in detail in [26]. The diameter of CNTs grown this way ranges from 1 to 4 nm as measured with an AFM (Digital Instruments, Multimode).

3.2.3.2 Source and Drain Contacts

An SEM (Hitachi 4700) was used to locate the CNTs and the catalyst pattern was used an alignment marker to align metal contacts to the CNTs. Source and drain electrodes made of Ti/Au thin film was achieved by conventional optical lithography. The scaling limit of the length of the CNTs from source to drain was only subject to the resolution of the lithography system. After depositing source and drain electrodes, a SEM was employed again to identify the number of CNTs in between.

3.2.3.3 Silicon Nitride Thin Film Deposition

Silicon nitride thin film was deposited from SiH_4 and NH_3 in a high purity N_2 carrier gas at 225 °C by PECVD (Plasma-Therm Model 790). The software interface of Plasmas-Therm Model 790 allowed easy control of the thickness of gate dielectric. For comparison, a SiO_2 thin film was also deposited on similar samples from SiH_4 and N_2O under the same conditions.

The exact film thickness was determined by an ellipsometer. Reactive ion etching (RIE), also built on the Plasma-Therm Model 790, was then utilized for opening holes in

the silicon nitride to the source and drain electrodes. The gate electrode was defined using optical lithography. In Figure 3.2, the CNT is illustrated to be only partially gated. However, the real devices made from the same wafer adopted two different designs – full gate and partial gate. For the fully gated transistors, gate electrode is deposited to exactly overlap the gap between source and drain. For the partial gate, metal electrode overlaps only the middle part of the CNT between source and drain and the segment of CNT not gated is 2 μm on each side. The schematic fabrication sequence is depicted in Figure 3.3.

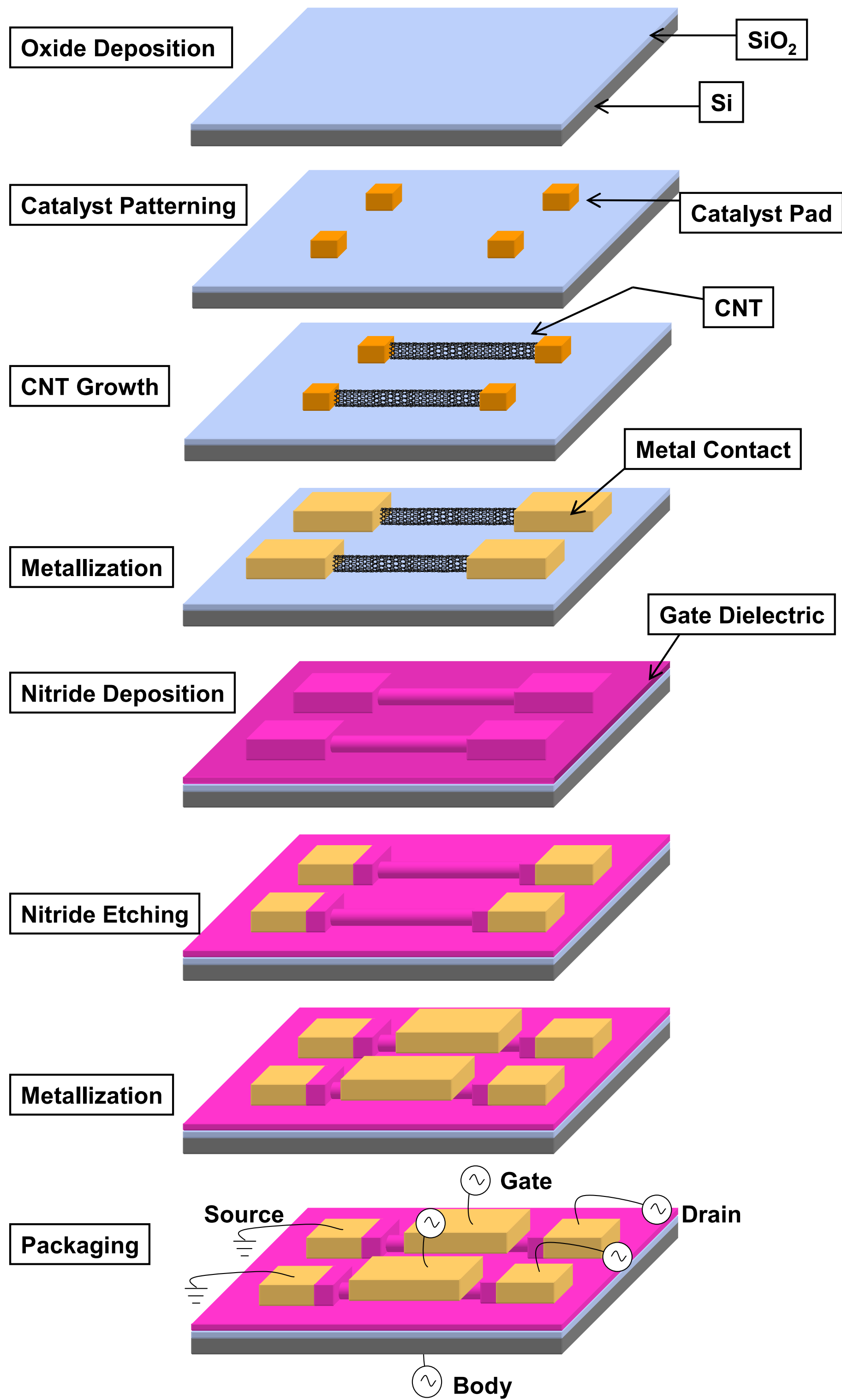

Figure 3.3 Detailed processing steps.
(not to scale)

3.2.4 Electrical Measurement and Discussion

Electrical transport measurements were carried out at room temperature and 4 K of more than 50 Si_3N_4/CNT and SiO_2/CNT transistors obtained from devices fabricated during various CNT growth and dielectric thin film deposition runs. Small bias source-drain conductance is non zero at room temperature, suggesting that as-grown CNT might be doped during the process [34]. In-depth investigation of partially gated CNT FETs is still beyond the scope of this thesis. In the following paragraph, only devices with full gate will be discussed.

We observed Schottky barrier behavior for our Si_3N_4/CNT samples with full-gate. at room temperature, shown in Figure 3.4 (a). The energy barriers became more pronounced at 4 K, where the thermal energy of charge carriers was significantly less than that at room temperature. Figure 3.4 (b) illustrates an I-V curve measured for the same sample in Figure 3.4 (a) at 4 K. The barrier is observed to be 0.15 V. The gating effect beyond the barrier revealed the dominant charge carriers are p-type. The Schottky barrier behavior visible is present both before and after deposition of the silicon nitride. Reference [43] argues that these barriers result from the work function difference between the CNT and metal contacts. A detailed microscopic theory of the interaction of CNTs with Si_3N_4 is still needed. In contrast to Si_3N_4/CNT samples, the source-drain electrical conduction disappeared for all the SiO_2/CNT samples. This is not surprising considering the fact that various oxygen related species prevalent during the deposition of SiO_2 are radicals or excited molecules, which readily destroyed CNTs by chemical reaction. This prompted us to look for an oxygen-free dielectric material.

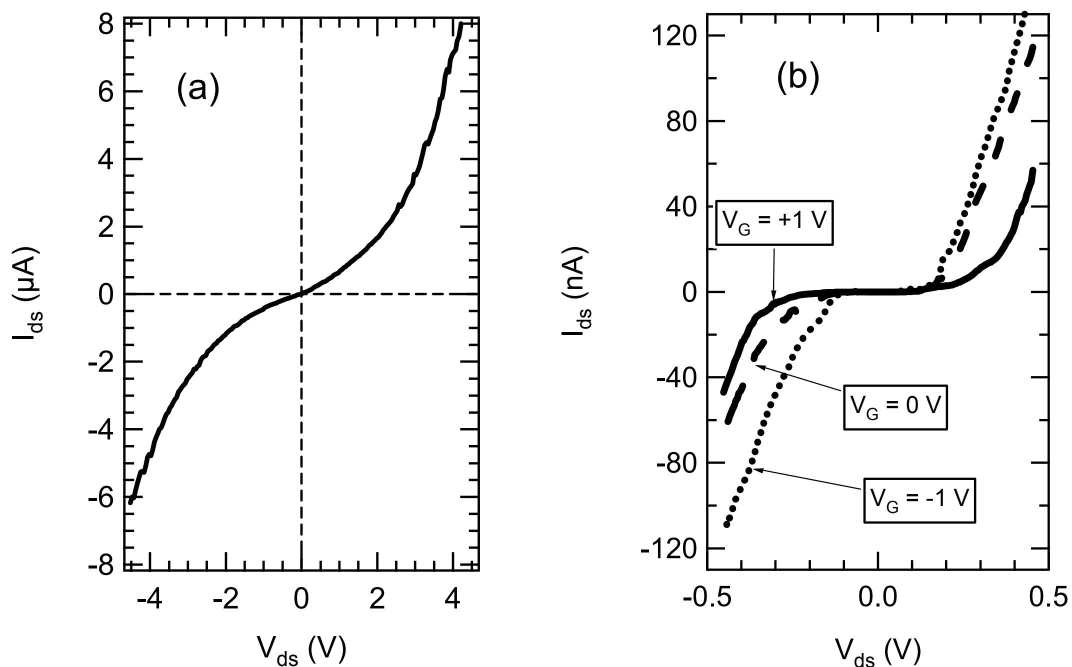

Figure 3.4 I-V characteristics of a top-gated CNTFET using silicon nitride gate dielectric.

(a) Room temperature (Vg = 0 V), (b) 4 K (varied Vg)
(dielectric thickness 50 nm; gate length 10 µm)

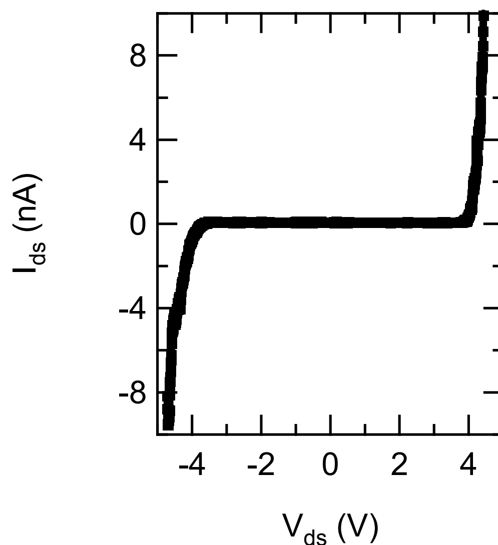

Figure 3.5 I-V characteristics (Vg = 0V) of a top-gated CNTFET.

(dielectric thickness 50 nm; gate length 10 µm; 4 K). This sample was annealed in argon at 600 °C for 5 minutes before electrical measurement.

At the moment, the dc/ac performance of our Si_3N_4/CNT transistors is severly suppressed by the presence of Schottky barrier at the metal/CNT interface. Figure 3.5 shows the I-V curve of another sample with a barrier nearly 4 V, corresponding to the reverse breaking-down voltage of a Schottky junction. While we carried out annealing in argon at 600 °C attempting to improve the quality of the CNT/metal contact, the improvement was not significant. The gating effect is not pronounced and the reason may be that the metal/CNT contact is very poor and the contact barrier is too high. Recent progress with respect to the CNT/metal contact has been made using Pd as source and drain electrodes [12]. There, the contact resistance approached the quantum limit and ballistic transport was observed. Combining Pd contacts with Si_3N_4 dielectric is clearly a topic for future research. The other factor that limits the performance of as-obtained Si_3N_4/CNT transistors is the length of the CNT between source and drain and the thickness of the nitride. Considering the current dielectric thickness of 50 nm and gate length of 10 μm, there is still plenty of room for improvement. For example, more advanced thin film deposition techniques such as ALD and JVD instead of PECVD can be used to fabricate thinner dielectrics. In addition, short length devices may achieve higher transconductance.

In summary, a process of fabricating top-gated CNT FETs using silicon nitride as gate dielectric has been demonstrated and silicon nitride is found to be chemically benign to CNTs. Our work represents the first demonstration of gating a nanotube with an oxygen free dielectric. Next phase of the research will focus on improving the performance of Si_3N_4 gated CNT FETs. Our goal is to achieve high speed devices and circuits based on CNTs.

CHAPTER 4

CARBON NANOTUBE GHZ DEVICES

The dynamical electrical properties of CNTs are technologically relevant for high speed electronic devices and circuits based on CNTs. At dc, it is known that electrons can move without scattering over microns inside a CNT [44]. The dynamical properties of nanotubes may be quite different than the dc properties, due to the quantum nature of electrons confined to one dimension.

In this chapter, we present the first microwave measurements of the dynamical impedance of electrically contacted individual single-walled CNTs. In order to measure the source-drain ac current and voltage at microwave frequencies, we constructed a resonant LC impedance matching circuit at 2.6 GHz. Both semiconducting and metallic CNTs are measured. Varying the back-gate voltage for a semiconducting CNT at dc varies the 2.6 GHz source-drain impedance. In contrast, varying the back-gate voltage on a metallic CNT at dc has no effect on the microwave source-drain impedance. We find that the ac source-drain impedance to be different than the dc source-drain resistance, which may be due to the distributed nature of the capacitive and inductive impedance of the contacts to the CNT and the CNT itself.

The geometry and fabrication of these devices are described in the first section. In the second section, measurements of the semiconducting CNT are analyzed and discussed. In the third section, measurements of the metallic CNT are analyzed and discussed.

4.1 Device Fabrication

4.1.1 CNT Growth

The CNTs were grown from lithographically patterned nanoparticle catalyst sites using CVD. The nanotube growth procedure and recipes are described in details in Chapter 2 and reference [26].

4.1.2 Electrical Contact

Electrical contact was achieved with evaporated Ti/Au electrodes using self-marked photolithography as presented in Chapter 3. Ti (200 Å) and Au (1000 Å) were deposited by electron beam evaporator. An SEM was used to locate the nanotubes before the electrical contact, and the catalyst pattern was used to align the contacts to the nanotubes. This self-marked process is also discussed in Chapter 3. The metallic CNT was annealed at 600 °C in Ar for 5 minutes; the semiconducting nanotube was not annealed. The electrode pattern consisted of a ~ 1 mm by ~ 1 mm contact pad.

4.1.3 Device Characterization

SEM (Hitachi 4700) images of two CNT devices are shown in Figure 4.1 and 4.2. The metallic CNT is ~ 60 μm in length (See reference [26]) and metal electrodes covered it more than 20 μm on each end. The semiconducting CNT is about 40 μm in length

(SEM image not shown here) and it was covered by the ~ 15 μm on the left side and ~ 10 μm on the other side. The lift-off the semiconducting CNT sample was not perfect with irregular edges on both sides. In addition, there is another short CNT protruding from the right electrode. Fortunately, it doesn't reach the left electrode, as justified by both SEM and AFM (Digital Instruments, Multimode) images (not shown).

Both devices were fabricated simultaneously on the same wafer and were only separated by cleaving after the fabrication process. This means they were both grown in the same growth run, the metallization was evaporated onto both samples in the same metallization procedure, etc. The diameter of nanotubes grown under similar conditions in our lab was less than 1.5 nm as measured with an AFM (Digital Instruments, Multimode), which leads us to conclude that the nanotubes shown are single-walled nanotubes.

4.2 LC Resonator Design

The microwave reflection coefficient ($S_{11} = \frac{Z_L - Z_0}{Z_L + Z_0}$, where Z_0 is the characteristic impedance of the transmission line and Z_L is the load impedance) was measured off of an LC resonator fabricated out of the nanotube mounted to a test fixture. The wire bonds used to connect the device served as the inductor, and the on-chip capacitance to ground served as the capacitor. We performed measurements at room temperature and at 4 K. At room temperature, the substrate losses were severe. Therefore, only the 4 K data will be presented in the following.

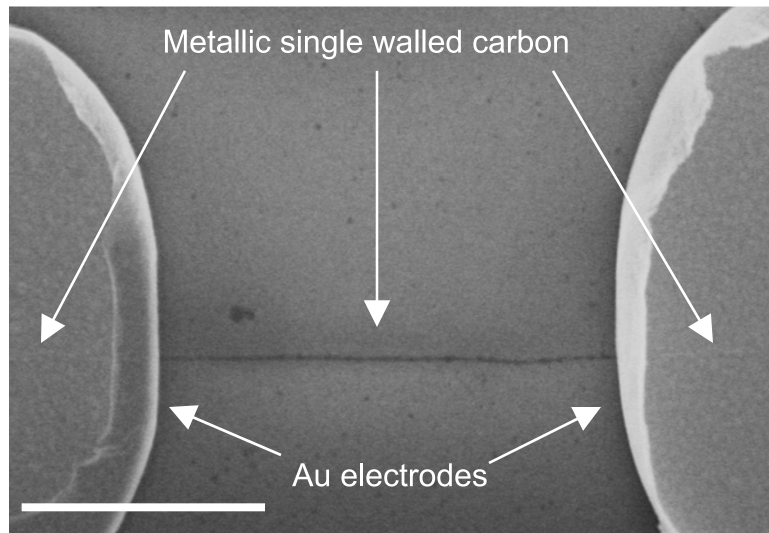

Figure 4.1 SEM image of the metallic single-walled CNT.
CNT underneath the electrodes is also shown. Scale bar: 5 μm.

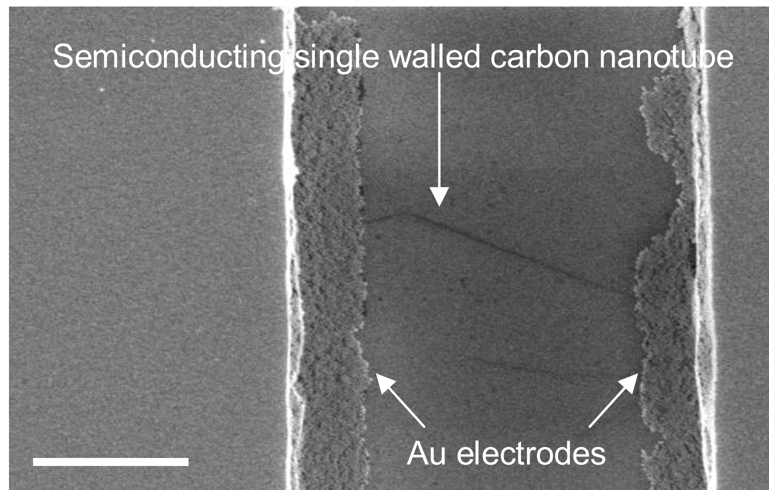

Figure 4.2 SEM image of the semiconducting single-walled CNT.
CNT underneath the electrodes is hard to see in this SEM image. Scale bar: 5 μm

4.2.1 Test Fixture

A microstrip launcher was used to connect an SMA cable to a 1 cm length of Cu microstrip on a 0.5 mm thick Duroid substrate (Z_0 = 50 Ω). The test fixture used was characterized extensively in reference [24]. There, it was shown to provide resonance free performance up to 40 GHz. For the measurements at 4 K, a 1 m long UT-141 cable was used to insert the test fixture directly into a liquid He storage dewar.

4.3.2 Device Mounting

The Si wafer with the nanotube devices was cleaved into 2 x 2 mm pieces, and abutted to the end of the microstrip. The plane of the microstrip and the surface of the Si wafer were at the same height above the brass test fixture. Because the substrate was used as a gate and the test fixture was grounded, we used a thin piece of Cu tape on the back side of the substrate to provide electrical contact to the substrate but to insulate the substrate from ground.

To contact the sample electrically, 25 μm diameter gold wires of length ~ 2 cm were soldered from the end of the microstrip to one of the electrical contact pads (Drain), and from the other electrical contact pad (Source) to the ground plane. These provided the inductors which formed approximately 10 nH of inductance in series with the nanotube. When we measured the same sample mounted with In solder (which has very little inductance) instead of wire bonds, the resonance dip in S_{11} (see below) disappeared, thus verifying that the Au wires served as inductors. The excess capacitance to ground from the electrical contact pads is estimated to be ~ 0.1 pF from the geometry.

4.3.3 Equivalent Circuit

The equivalent LC matching circuit is depicted in Figure 4.3. We measured S_{11} off of this resonator using a control sample with the same electrode pattern as the CNT device (but no CNT), and found there is still a dissipation in the resonator, i.e. a finite Q. We attribute this radiation loss into free space from the wires. Numerically, this radiation resistance is ~ 10 kΩ and varies with the length of the wire used. This issue will be further quantified in future work on optimized resonator design.

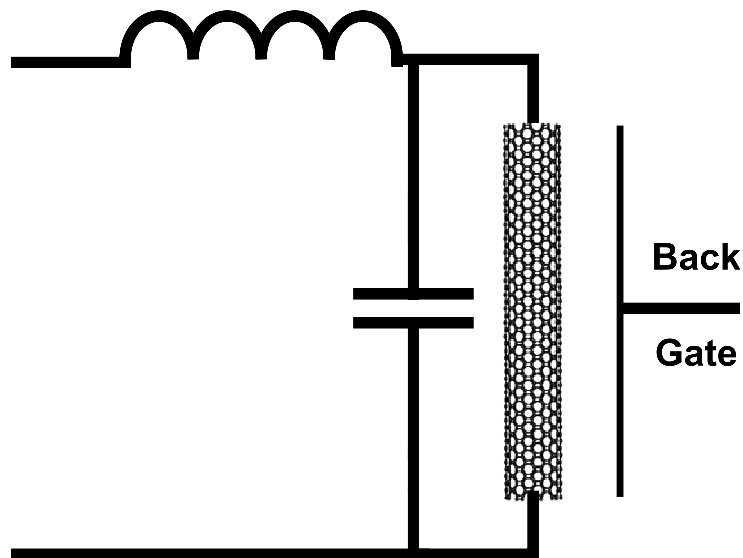

Figure 4.3 Equivalent circuit for the resonator.

4.3 Semiconducting CNT Resonator

4.3.1 Semiconducting CNT DC Electrical Properties

The semiconducting CNT had a room temperature resistance of 300 kΩ (Vg = 0 V), and behaved as a p-type device when using the substrate as a back-gate, consistent with previously measured results [44]. Because the CNT could be gated at room temperature, we have characterized it as a semiconducting CNT.

At 4 K, the dc performance is more complicated. We plot in Figure 4.4 the low-bias source-drain conductance vs. back-gate voltage. The complicated structure is probably due to a combination of Coulomb-blockade (single electron transistor) effects and quantum interference of the electron wave functions. The inset shows the nanotube I-V curve, which shows a gap at the origin. Complicating the issue is the fact that the semiconducting CNT is not straight (see Figure 4.2), and so may behave as a series of quantum dots at 4 K. At room temperature, the depletion curve was smooth, without fine structure.

A critical issue is how the nanotube contacts the Au electrically. At dc, the theoretical lower limit for the CNT resistance is $R_0 = h/4e^2 \approx 6.5$ k Ω. At ac, the theory is much more complicated. For the CNTs we present in this work, the CNT extended under the Au contact pads by more than 10 μm on each side. Thus, even though the dc contact resistance is high (~ 1 M Ω, see below), there may be an additional capacitive electrical contact to the CNT, if the evaporated Au does not destroy the nanotube. Indeed, other

SEM and AFM images (not shown) indicate the nanotube is still intact under the Au electrodes.

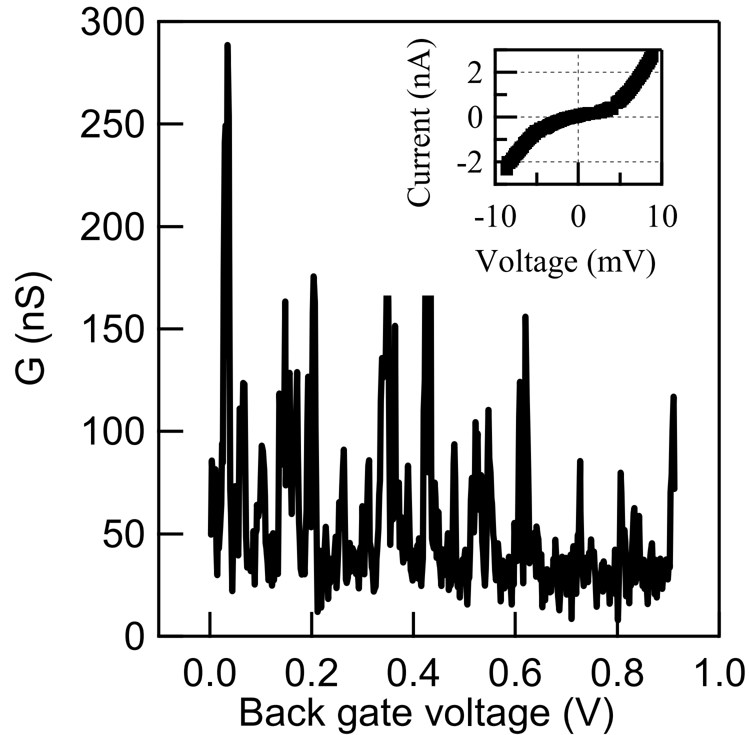

Figure 4.4 DC electrical properties of semiconducting CNT.

4.3.2. Semiconducting CNT AC Electrical Properties

In Figure 4.5 we show the measured S_{11} vs. frequency for the semiconducting nanotube. A clear resonance is visible at 2.6 GHz, where the impedance matching circuit transforms the nanotube impedance to ~ 50 Ω. By applying a voltage of 10 Vpp to the substrate, we are able to consistently change the measured value of S_{11} on resonance with high reproducibility, as shown in the inset. This clearly demonstrates that varying the

gate voltage at dc varies the 2.6 GHz source-drain impedance, thus verifying microwave frequency operation of a CNT transistor.

From a RF circuit designer's point of view, we also demonstrated a CNT GHz nano-resonator with Q ~ 40, as determined by a 3 dB method. In addition, the Q of the semiconducting CNT resonator was tunable at microwave frequencies. This represents the first ever passive microwave circuit component based on CNTs.

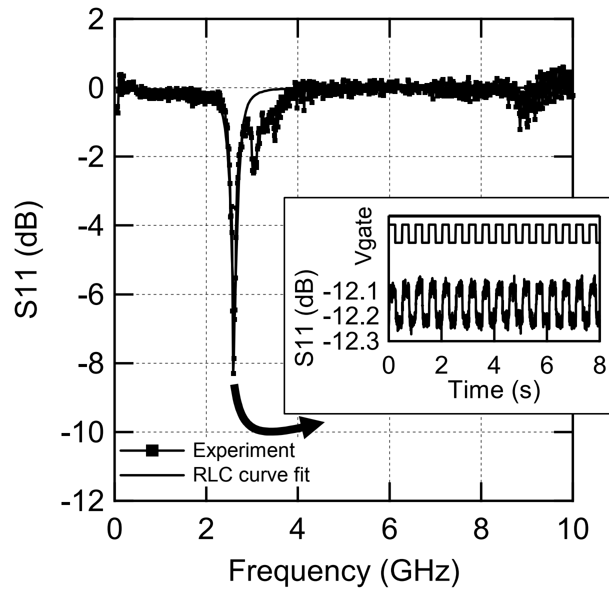

Figure 4.5 Measured S_{11} for semiconducting nanotube resonator.
The time domain measurement is exactly on resonance, where as the frequency domain measurement missed the resonance frequency due to the finite point density.

4.3.4. Analysis and Discussion

The ac impedance of a CNT should have significant real and imaginary components. In this work, the inductance in our matching circuit is set by the length of the wire bond, which is only approximately known. Thus we can not quantitatively determine which part of the inductance is due to the CNT, and which part is due to the

wire bond. This issue will be addressed in future work with lithographically fabricated, integrated matching circuits. If we model the CNT as shown in Figure 4.3 as a pure resistor, a three parameter fit to the measured S_{11} data give values of L = 40 nH, C = 0.1 pF, and R = 27 kΩ. (The fitted curve is also shown in Figure 4.5) The fitted resistance is comparable to the radiation resistance for this circuit, indicating that the CNT ac resistance is presumably much larger. This is consistent with the measured dc resistance of ~ 5 MΩ (Vg = 0 V) at 4 K.

We would like to correlate the nanotube ac performance with its dc electrical properties. If we assume the dc resistance of the nanotube is the same as the ac resistance of the nanotube, then the effect of the gate voltage is to change the CNT ac resistance from ~ 3 MΩ to > 20 MΩ, as can be seen from Figure 4.4.

For the microwave measurements, the radiation resistance (~ 27 kΩ) is independent of the gate voltage. Since the radiation resistance is in parallel with the nanotube resistance, the effect of the gate voltage is to modulate the resistance by ~ [(27 kΩ ||20MΩ) – (27 kΩ ||3 MΩ)] ~ 100 Ω. This is numerically about a factor of 10 smaller than the observed change in S_{11} of 0.1 dB. Thus the nanotube ac electrical properties are different than the dc electrical properties. Possible reasons for this are discussed below.

4.4 Metallic CNT Resonator

4.4.1 Metallic Nanotube DC Electrical Properties

The metallic nanotube had a room temperature resistance of 80 kΩ; this did not vary appreciably (less than 1%) with a back-gate voltage. Because the nanotube could not be gated at room temperature, we have characterized it as a metallic nanotube. We plot in Figure 4.6 the conductance vs. gate voltage at 4 K, where it is seen that the CNT conductance is independent of gate voltage. The I-V curve (also shown in Figure 4.6) is linear.

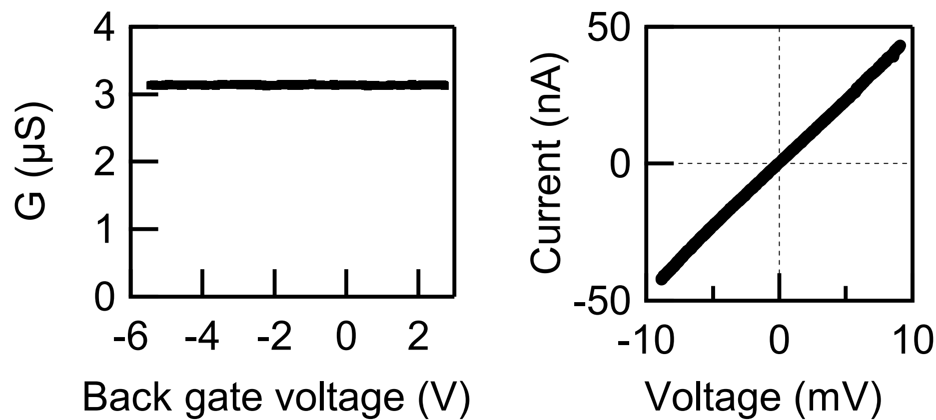

Figure 4.6 DC electrical properties of metallic nanotube.

4.4.2 Metallic Nanotube AC Electrical Properties

In Figure 4.7 we plot the measured S_{11} vs. frequency for the metallic CNT. A clear resonance is visible at 4 GHz, where the impedance of the CNT is transformed

down to close to 50 Ω. The resonance frequency is slightly different due to the different length of wire used to mount this sample. In contrast to the semiconducting CNT resonator, a voltage of 10 Vpp applied to the substrate does not change the S_{11} within the noise limits of 0.01 dB. If we model the CNT as shown in Figure 4.7 as a pure resistor, a 3 parameter fit to the measured S_{11} data give a value of L = 14 nH, C = 0.1 pF, and R = 1.7 kΩ. The fitted curve is also shown in Figure 4.7. The resistance is lower than the radiation resistance, indicating that the nanotube ac resistance is indeed 1.7 kΩ. This is significantly different than the CNT dc resistance.

Neither the dc nor ac properties of the metallic nanotube depend on the back-gate voltage. In this sense, the dc and ac electrical properties are consistent. However, the absolute dc and ac electrical resistances are different.

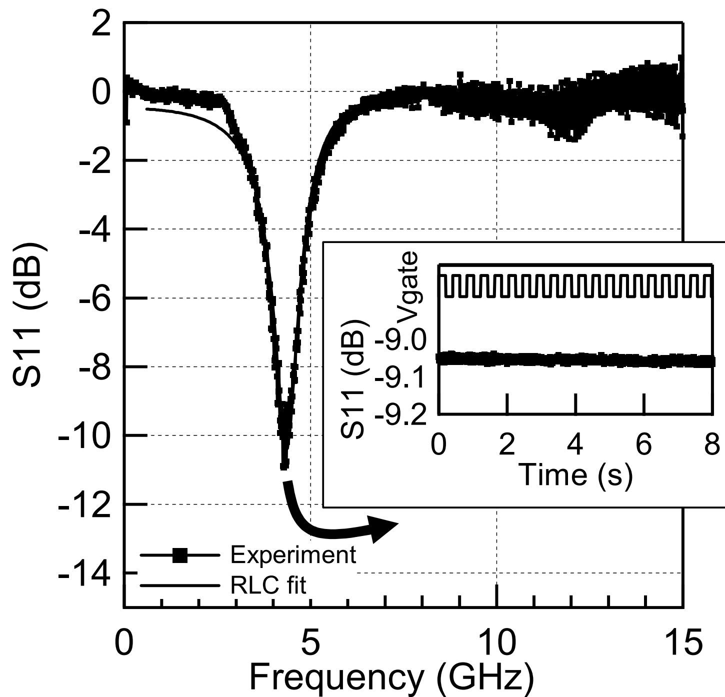

Figure 4.7 Measured S_{11} for metallic nanotube resonator.

4.4.3. Analysis and Discussion

We now discuss possible reasons for the difference between the measured dc and ac impedance. For the metallic CNT in particular, the inferred resistance at ac is less than the theoretical Landauer-Buttiker formalism lower limit of $h/4e^2$. This is not an inconsistency with theory. Indeed, it is possible for a capacitively contacted CNT (or more generally, a 1D conductor) with no scattering in the channel to have an ac impedance which is less than $h/4e^2$, because there is no contact resistance if the contact is solely capacitive. From a theoretical point of view, if there is no scattering along the CNT length and the CNT is capacitively contacted, then at ac there should be no dissipation at all. While we did not emphasize this point explicitly, reference [22] and [23] provided extensive modeling of the effects of the distributed capacitive contacts on a CNT. In our devices, there is clearly some dc contact resistance, but in addition there may be significant capacitive coupling because the CNT extends under the contacts by approximately 20 μm on each side. The metal was evaporated directly onto the CNT so the capacitive coupling should be very strong.

4.5 Conclusion and Future Work

We have clearly demonstrated the operation of a nanotube transistor at microwave frequencies[45]. Nonetheless, we have not fully characterized all of the ac properties. A full characterization would require measurements of the source-drain ac current, the source-drain ac voltage, the gate-source ac current, the gate-source ac voltage, and their relationship (a 2×2 matrix called h-matrix, or equivalently the impedance matrix, or equivalently the S matrix), all as functions of the dc gate bias, the dc drain bias and frequencies. What we have measured here is the ratio of the ac source-drain voltage to the ac source-drain current at microwave frequencies, and showed that it depends on the dc gate voltage. These full characterization measurements, although challenging because of the high impedances involved, are clearly a topic for future research.

As well, CNT GHz nano-resonators have been achieved in this work. The Q of the nano-resonator based on semiconducting CNTs can be tuned by modulating the back-gate voltage. This shed light on both passive and active RF/microwave signal processing components based on CNTs.

APPENDIX A NANO FURNACE MANUAL

Note about safety: No Guarantee.

- **This manual is only a summary checklist.**
- **In person training is necessary to ensure safe operation.**

1. Check in:

a) Gas sensor should be on and the readout displays 0% LEL normally.
b) The control power for the front panel should be on and in the constant voltage mode: 24 V.
c) Make sure N_2 is turned on, Tylan readout =150 sccm.
d) Push "TEST" on the front panel to make sure all the gas switches are working properly.

2. Operation:

1) Switch the cable connecting N_2 MKS and Tylan to Ar MKS.
2) Open the Ar regulator on the top of the cylinder. Turn on Ar to set the flow rate at 1500 sccm.
3) Turn off N_2.
4) Load your samples.
5) Turn on the furnace controller; run the predefined temperature program. **(Don't change the program without permission).**
6) Keep flowing Ar and the temperature of the growth tube should have reached 900 °C. The temperature ramping and dwelling takes about 30 minutes.
7) Make sure the temperature is stable at 900 °C.
8) Open the regulator on the top of the H_2 cylinder, record this pressure in the log-in sheet.
9) Turn on H_2. Set the H_2 flow rate to be 200 sccm.
10) Check the gas leakage using the portable gas detector. If normal, turn off Ar.
11) Keep flowing H_2 at 200 sccm for 5 minutes.
12) Open the regulator on the top of the CH_4 cylinder, record the pressure in the log-in sheet.
13) Turn on CH_4 and set the flow rate to be 1000 sccm.
14) Keep flowing 10 ~ 15 minutes. Don't exceed 15 minutes.

15) At the end of active growth, the temperature of the growth tube starts to drop. Turn off CH_4.
16) Turn on Ar (1500 sccm).
17) Turn off H_2.
18) Record the CH_4 pressure and then close the regulator on the top of the CH_4 cylinder.
19) Record the H_2 pressure and then close the regulator on the top of the H_2 cylinder.
20) When the temperature of the growth tube drops to 200 °C, Turn off Ar and switch back to N_2 (150 sccm).
21) Record the Ar pressure and then close the regulator on the top of the cylinder.
22) Let the system cool down to room temperature and then take out your sample. It generally takes more than 3 hours for the system to cool down to room temperature.
23) Clean the joint between the end cap the growth tube and gently rejoin them.

3. Check out

1) Turn off the furnace controller.
2) Double check that you have closed all the gas regulators.
3) Sign the log-in sheet and submit it to Sheldon.

REFERENCE

[1] S. Iijima, "Helical Microtubules of Graphitic Carbon," *Nature*, vol. 354, pp. 56-58, 1991.

[2] G. D. Mildred S. Dresselhaus, Phaedon Avouris, Eds., *Carbon nanotubes: synthesis, structure, properties, and applications*. Berlin, Germany: Springer-Verlag, 2001.

[3] T. W. Ebbesen and P. M. Ajayan, "Large-Scale Synthesis of Carbon Nanotubes," *Nature*, vol. 358, pp. 220-222, 1992.

[4] D. S. Bethune, C. H. Kiang, M. S. Devries, G. Gorman, R. Savoy, J. Vazquez, and R. Beyers, "Cobalt-Catalyzed Growth of Carbon Nanotubes with Single-Atomic-Layerwalls," *Nature*, vol. 363, pp. 605-607, 1993.

[5] A. Thess, R. Lee, P. Nikolaev, H. J. Dai, P. Petit, J. Robert, C. H. Xu, Y. H. Lee, S. G. Kim, A. G. Rinzler, D. T. Colbert, G. E. Scuseria, D. Tomanek, J. E. Fischer, and R. E. Smalley, "Crystalline ropes of metallic carbon nanotubes," *Science*, vol. 273, pp. 483-487, 1996.

[6] J. Kong, H. T. Soh, A. M. Cassell, C. F. Quate, and H. J. Dai, "Synthesis of individual single-walled carbon nanotubes on patterned silicon wafers," *Nature*, vol. 395, pp. 878-881, 1998.

[7] S. Datta, *Electronic Transport in Mesoscopic Systems*. Cambridge, U.K.: Cambridge Univ. Press, 1995.

[8] J. Kong, E. Yenilmez, T. W. Tombler, W. Kim, H. J. Dai, R. B. Laughlin, L. Liu, C. S. Jayanthi, and S. Y. Wu, "Quantum interference and ballistic transmission in nanotube electron waveguides," *Physical Review Letters*, vol. 87, pp. 106801, 2001.

[9] W. J. Liang, M. Bockrath, D. Bozovic, J. H. Hafner, M. Tinkham, and H. Park, "Fabry-Perot interference in a nanotube electron waveguide," *Nature*, vol. 411, pp. 665-669, 2001.

[10] S. Heinze, J. Tersoff, R. Martel, V. Derycke, J. Appenzeller, and P. Avouris, "Carbon nanotubes as Schottky barrier transistors," *Physical Review Letters*, vol. 89, pp. 106801, 2002.

[11] F. Leonard and J. Tersoff, "Role of Fermi-level pinning in nanotube Schottky diodes," *Physical Review Letters*, vol. 84, pp. 4693-4696, 2000.

[12] A. Javey, J. Guo, Q. Wang, M. Lundstrom, and H. J. Dai, "Ballistic carbon nanotube field-effect transistors," *Nature*, vol. 424, pp. 654-657, 2003.

[13] T. Durkop, S. A. Getty, E. Cobas, and M. S. Fuhrer, "Extraordinary mobility in semiconducting carbon nanotubes," *Nano Letters*, vol. 4, pp. 35-39, 2004.

[14] S. Frank, P. Poncharal, Z. L. Wang, and W. A. de Heer, "Carbon nanotube quantum resistors," *Science*, vol. 280, pp. 1744-1746, 1998.

[15] S. Rosenblatt, Y. Yaish, J. Park, J. Gore, V. Sazonova, and P. L. McEuen, "High performance electrolyte gated carbon nanotube transistors," *Nano Letters*, vol. 2, pp. 869-872, 2002.

[16] J. Guo, M. Lundstrom, and S. Datta, "Performance projections for ballistic carbon nanotube field-effect transistors," *Applied Physics Letters*, vol. 80, pp. 3192-3194, 2002.

[17] J. Guo, S. Goasguen, M. Lundstrom, and S. Datta, "Metal-insulator-semiconductor electrostatics of carbon nanotubes," *Applied Physics Letters*, vol. 81, pp. 1486-1488, 2002.

[18] A. Bachtold, P. Hadley, T. Nakanishi, and C. Dekker, "Logic circuits with carbon nanotube transistors," *Science*, vol. 294, pp. 1317-1320, 2001.

[19] X. L. Liu, C. Lee, C. W. Zhou, and J. Han, "Carbon nanotube field-effect inverters," *Applied Physics Letters*, vol. 79, pp. 3329-3331, 2001.

[20] A. Javey, Q. Wang, A. Ural, Y. M. Li, and H. J. Dai, "Carbon nanotube transistor arrays for multistage complementary logic and ring oscillators," *Nano Letters*, vol. 2, pp. 929-932, 2002.

[21] H. W. C. Postma, T. Teepen, Z. Yao, M. Grifoni, and C. Dekker, "Carbon nanotube single-electron transistors at room temperature," *Science*, vol. 293, pp. 76-79, 2001.

[22] P. J. Burke, "Luttinger liquid theory as a model of the gigahertz electrical properties of carbon nanotubes," *IEEE Transactions on Nanotechnology*, vol. 1, pp. 129-144, 2002.

[23] P. J. Burke, "An RF circuit model for carbon nanotubes," *IEEE Transactions on Nanotechnology*, vol. 2, pp. 55-58, 2003.

[24] P. J. Burke, I. B. Spielman, J. P. Eisenstein, L. N. Pfeiffer, and K. W. West, "High frequency conductivity of the high-mobility two-dimensional electron gas," *Applied Physics Letters*, vol. 76, pp. 745-747, 2000.

[25] H. C. Choi, S. Kundaria, D. W. Wang, A. Javey, Q. Wang, M. Rolandi, and H. J. Dai, "Efficient formation of iron nanoparticle catalysts on silicon oxide by hydroxylamine for carbon nanotube synthesis and electronics," *Nano Letters*, vol. 3, pp. 157-161, 2003.

[26] S. Li, Z. Yu, G. Gadde, P. J. Burke, and W. C. Tang, "Carbon nanotube growth for GHz devices," *Proceedings of the 3rd IEEE Conference on Nanotechnology*, vol. 2, pp. 256-258, 2003.

[27] T. Brintlinger, Y. F. Chen, T. Durkop, E. Cobas, M. S. Fuhrer, J. D. Barry, and J. Melngailis, "Rapid imaging of nanotubes on insulating substrates," *Applied Physics Letters*, vol. 81, pp. 2454-2456, 2002.

[28] P. M. Campbell, E. S. Snow, and J. P. Novak, "Simple catalyst for the growth of small-diameter carbon nanotubes," *Applied Physics Letters*, vol. 81, pp. 4586-4588, 2002.

[29] Y. G. Zhang, A. L. Chang, J. Cao, Q. Wang, W. Kim, Y. M. Li, N. Morris, E. Yenilmez, J. Kong, and H. J. Dai, "Electric-field-directed growth of aligned single-walled carbon nanotubes," *Applied Physics Letters*, vol. 79, pp. 3155-3157, 2001.

[30] Y. Huang, X. F. Duan, Q. Q. Wei, and C. M. Lieber, "Directed assembly of one-dimensional nanostructures into functional networks," *Science*, vol. 291, pp. 630-633, 2001.

[31] J. Liu, M. J. Casavant, M. Cox, D. A. Walters, P. Boul, W. Lu, A. J. Rimberg, K. A. Smith, D. T. Colbert, and R. E. Smalley, "Controlled deposition of individual single-walled carbon nanotubes on chemically functionalized templates," *Chemical Physics Letters*, vol. 303, pp. 125-129, 1999.

[32] S. J. Tans, A. R. M. Verschueren, and C. Dekker, "Room-temperature transistor based on a single carbon nanotube," *Nature*, vol. 393, pp. 49-52, 1998.

[33] S. J. Wind, J. Appenzeller, R. Martel, V. Derycke, and P. Avouris, "Vertical scaling of carbon nanotube field-effect transistors using top gate electrodes," *Applied Physics Letters*, vol. 81, pp. 1359-1359, 2002.

[34] A. Javey, H. Kim, M. Brink, Q. Wang, A. Ural, J. Guo, P. McIntyre, P. McEuen, M. Lundstrom, and H. J. Dai, "High-kappa dielectrics for advanced carbon-nanotube transistors and logic gates," *Nature Materials*, vol. 1, pp. 241-246, 2002.

[35] P. G. Collins, K. Bradley, M. Ishigami, and A. Zettl, "Extreme oxygen sensitivity of electronic properties of carbon nanotubes," *Science*, vol. 287, pp. 1801-1804, 2000.

[36] V. Derycke, R. Martel, J. Appenzeller, and P. Avouris, "Controlling doping and carrier injection in carbon nanotube transistors," *Applied Physics Letters*, vol. 80, pp. 2773-2775, 2002.

[37] T. P. Ma, "Making silicon nitride film a viable gate dielectric," *IEEE Transactions on Electron Devices*, vol. 45, pp. 680-690, 1998.

[38] Y. Shi, X. W. Wang, and T. P. Ma, "Electrical property of high-quality ultrathin nitride/oxide stack dielectrics," *IEEE Transactions on Electron Devices*, vol. 46, pp. 362-368, 1999.

[39] K. A. Nasyrov, V. A. Gritsenko, A. K. Kim, H. S. Chae, S. D. Chae, W. I. Ryu, J. H. Sok, J. W. Lee, and B. M. Kim, "Charge transport mechanism in metal-nitride-oxide-silicon structures," *IEEE Electron Device Letters*, vol. 23, pp. 336-338, 2002.

[40] A. Nakajima, T. Yoshimoto, T. Kidera, and S. Yokoyama, "Low-temperature formation of silicon nitride gate dielectrics by atomic-layer deposition," *Applied Physics Letters*, vol. 79, pp. 665-667, 2001.

[41] M. Gupta, V. K. Rathi, R. Thangaraj, O. P. Agnihotri, and K. S. Chari, "The Preparation, Properties and Applications of Silicon-Nitride Thin-Films Deposited by Plasma-Enhanced Chemical Vapor-Deposition," *Thin Solid Films*, vol. 204, pp. 77-106, 1991.

[42] Z. F. Ren, Z. P. Huang, J. W. Xu, J. H. Wang, P. Bush, M. P. Siegal, and P. N. Provencio, "Synthesis of large arrays of well-aligned carbon nanotubes on glass," *Science*, vol. 282, pp. 1105-1107, 1998.

[43] S. Heinze, J. Tersoff, R. Martel, V. Derycke, J. Appenzeller, and P. Avouris, "Carbon nanotubes as Schottky barrier transistors," *Physical Review Letters*, vol. 89, pp. 106801-106804, 2002.

[44] P. L. McEuen, M. S. Fuhrer, and H. K. Park, "Single-walled carbon nanotube electronics," *IEEE Transactions on Nanotechnology*, vol. 1, pp. 78-85, 2002.

[45] S. Li, Yu, Z, Zhang, S, Burke, P, Tang, W, "Carbon nanotube transistor operation at 2.6 GHz," *Nano Letters*, vol. 4, pp. 753-756, 2004.